DESIGN AND DEVELOPMENT OF AN EFFICIENT COMPUTER SIMULATION MODEL FOR RESPONSE ANALYSIS OF A MOORED SEMI-SUBMERSIBLE

(DOI No. 10.3940/rina.ijme.2019.a1.503)

V Domala, Department of Petroleum Engineering and Earth Sciences, University of Petroleum and Energy Studies, Dehradun (UK), India and **R Sharma**, Design and Simulation Laboratory, Department of Ocean Engineering, IIT Madras, Chennai (TN), India.

SUMMARY

This paper presents the design and development of an efficient modular 'Computer Simulation Model (CSM)' for response analysis of a moored semi-submersible. The computer simulation model is designed in two split models (i.e. computational and experimental models) and each of these models consists of various modules. The modules are developed from basic governing equations related to motion and modules are integrated and we aim for a seamless integration. The moored semi-submersible is represented mathematically as six degrees of freedom dynamic system and the coupling effects between the structure and mooring lines are considered. The basic geometric configuration of semi-submersible is modelled and analyzed for stability computations in MS-Excel^{*TM} and then the basic governing equations related to motion are modelled mathematically in a module and solved numerically with Ansys-AQWA^{**TM}. The computational model is validated and verified with some available experimental results. The CSM is utilized to study the surge and sway responses with respect to the horizontal range of mooring lines and our results show good validation with the existing experimental results. Our presented results show that the fibre wires have minimum steady state response in surge and sway degrees of freedom as compared with the steel wires. However, they have large drift as compared with steel wires. Finally, we show that the computer simulation model can help in detailed analysis of responses and results can be utilized for design and development of new age semi-submersibles for optimum performances for a given set of parameters.

NOMENCLATURE

dof	Degree of freedom,
dofs	Degrees of freedom,
CoG	Centre of gravity,
A	Cross sectional area of mooring line,
a	Number of the pontoons,
b	Number of the columns,
C_{cs}	Added mass coefficient of the column in surge dof
C_{cw}	Added mass coefficient of the column in sway dof,
C_{ps}	Added mass coefficient of the pontoon in surge dof,
C_{pw}	Added mass coefficient of the pontoon in sway dof,
C_x and C_y	Damping coefficient in the directions of surge and sway dofs respectively.
E	Modulus of elasticity,
F_D	Diffraction force,
F_{FK}	Froude-Krylov force,
$F_{R_{ji}}$	Radiation force per unit wave amplitude,
B_{CG}	Buoyancy at the CoG,
h	Water depth,
H_s	Sub-merged draft of column,
$\hat{i}$	1 to n_m where n_m is the number of mooring lines,
K_{ij}	Stiffness matrix (for i , j = 1 to 2) in the translation dof,
M_a	Added mass of the structure,
M_s	Mass of the structure,
m_{a11}	Added mass in the surge dof,
m_{a22}	Added mass in the sway dof,
r	Radius of the semi-submersible column,
T_H	Horizontal component of the tension in mooring line,
$T_{\max}$	Maximum tension in the mooring line,
T_v	Vertical component of the tension in mooring line,
$T_{x\hat{i}}$	Initial horizontal tension of the mooring line in X - direction,
$T_{y\hat{i}}$	Initial horizontal tension of the mooring line in Y - direction,
$u_{\tilde{i}}$	where $\tilde{i}$ = 1 to $\hat{n}$ where $\hat{n}$ is number of peaks in logarithmic decay,
w	Submerged weight per unit length of the mooring line
X_R	Horizontal range between the fairlead and contact point on the sea bed,
Z_V	Vertical distance between the fairlead point on the structure and contact point on the sea bed,
ϕ_p	Velocity potential function,
ρ	Density of the sea water,
∇_p	Volume displaced by the pontoons,
ζ	Damping ratio,
Δx	Unit displacement in the X - direction,

Δy Unit displacement in the Y - direction,

ΔT_{xi} Change in the tension due to unit displacement in the X - direction, and

ΔT_{yi} Change in the tension due to unit displacement in the Y - direction.

1. INTRODUCTION

A semi-submersible is moored offshore floating structure used for exploring oil and gas in deepwater depths. Normally, because of low water plane area at the operating draft the motion responses of semi-submersible are low and it allows the use of semi-submersible over a wider range of weather and sea conditions. The motion response of semi-submersible depends on weight, draft, distance between pontoons, size of columns, wave direction, wave height and other parameters. Because of their industrial significance the motion response of semi-submersible has been studied by various researchers and research has focussed on variety of issues ranging from detailed computationally expensive numerical simulations to development of simple empirical formulations for design aid.

1.1 BACKGROUND AND MOTIVATION

The computation of motion response of semi-submersible is critically important for operation, survival and to ensure that exploratory drilling (main objective of using semi-submersible) continues with various wave heights and directions. In the literature, some experimental results are available that have been performed on model scale semi-submersibles for prediction of the motions, e.g. Takagi et al. (1985) presented detailed model results for all six degrees of freedom and discussed the effect of wave height and wave direction on heave motion, roll and pitch motion. However, their results are restricted to regular waves.

Kirk (1985) studied resonant heave response of semi-submersible and observed that the usages of square/rectangular shaped columns/pontoons with blunt edges in-place of circular/square/rectangular shaped columns/pontoons with rounded edges (either arc of a circle or ellipse) increases the drag coefficient but reduce the heave response. Furthermore, he observed that the non-linear drag force depends on column sizing and draft of the structure.

Later, van Santen (1985) proposed simple empirical formulas to compute the heave motion of semi-submersible and his results showed that the heave response depends on natural time period of heave and the submerged depth of pontoons or draft of the semi-submersible and on heave added mass. Sunil and Mukhopadhyay (1995) reported a detailed parametric study by varying the depth and dimensions of the floaters (i.e. pontoons) of semi-submersible.

Motions in the surge, sway and yaw degrees of freedom are important in operational performances of the semi-submersible because these dofs do not have the hydrostatic restoring force. The mooring lines provide restoring forces in these dofs and therefore they are critical in the unfavourable environmental conditions. In the absence of a restoring force, the motion response gets heavily dependent upon mooring lines and its properties. In this regard, we focus on semi-submersible as a moored floating structure and aim to study the interaction between the semi-submersible and mooring lines. The natural periods of surge, sway and yaw are dependent on mooring lines and properties of mooring line materials. The popular choices available for mooring lines are: steel wire, Aramid, polyester, High Modulus Poly Ethylene (HMPE) and chains, etc.

Yelmaz and Incecik (1996) discussed surge response with mooring line damping, without mooring line damping, with thrusters and without thrusters in moderate weather conditions and they concluded that the mooring line reduces the surge motion by around 43% and it is not altered by thrusters. For extreme weather conditions surge response reduction is around 5-7% with and without thrusters. Although, the thrusters and/or structure's own propeller system – Dynamic Positioning System (DPS) – can be and are used for motion control and maintain an offshore structure's position, they add to system complexity, high initial and operating costs, high chances of running off position by system/power failures, and underwater accidental hazards from thrusters for divers and the 'Remotely Operated Vehicles (ROVs)'. Hence, a solution based upon mooring lines is always preferred because of simplicity and economy.

Bowers et al. (1997) studied a multivariate, directional environmental force analysis on mooring lines to estimate the return period of mean mooring force. Brown and Mavrakos (1999) presented a comparative study on motion analysis of a structure with options of mooring line chain and mooring line wire at different water depths for harmonic and bi-harmonic waves using both the time and frequency domains methods for the prediction of maximum tension and mooring line damping. Their model was implemented in AQWA^{**TM}. Maeda et al. (2000) reported a time domain analysis on a very large floating structure with unidirectional and bi-directional irregular waves, and their experimental results were compared with theoretical results for vertical displacement and mooring line tension and showed good agreement. However, it is important to note here that the time domain simulation is computationally expensive than frequency domain simulation though it is more accurate. Madjid et al. (2011) reported an exhaustive code-to-code comparison for hydrodynamic motion of offshore wind turbine mounted on a spar platform, i.e. USFOS^{****TM} and HAWC2^{*****TM}, for more details see TMUSFOS (2015) and TMHAWC (2015). They focused on time domain simulations and their results - though computationally expensive with large running time - showed good agreements across code-to-

code for motion and tension responses. However, they did not focus on presenting a general simulation model that can be applied to an offshore structure for motion and tension responses and instead focused on specific example and what are the strengths and weaknesses of available software solutions?

Huijs (2007) studied the heave and horizontal motions of semi-submersible with catenary mooring and steel catenary risers and observed that the reaction force from motions perpendicular to the plane of riser are in smaller order than the reaction force from motions in the plane of the riser. Marcio and Celso (2007) reported a study on the behaviour of semi-submersible coupled with the drilling riser with dynamic positioning system and blow out preventer with current and waves. Also, a general simulation model needs to be verified and validated so that it can be applied to various design configurations. In general, the mooring line dynamics are studied with Finite Element Analysis (FEA) based methods and rod theory, e.g. Tahar and Kim (2008) presented case studies on classical spar with polyester mooring lines and on tensioned buoy with polyester wire and their approach is based on non-linear elastic rod theory. Song et al. (2010) studied the station keeping performance of semi-submersibles using different mooring materials such as HMPE, polyester and steel wires, and concluded that polyester mooring line are better option for deeper water. Tie-bing et al. (2011) presented an experimental investigation on a large volume semi-submersible to establish relationship between air-gap distributions, wave parameters and wave run-up characteristics on the aft to observed response. Huijs et al. (2014) presented aero-hydro-servo-elastic time domain simulations on tri floater semi-submersible with 5 MW NREL wind turbine using Ansys-AQWA^{**TM} coupled with PHATAS^{***TM} software (for more details see Lindenburg (2012)) to study the wind loads on turbine and wave loads on semi-submersible. Also, in their work the aero-hydro-servo-elastic time domain simulations are compared with uncoupled frequency domain analysis.

Yang et al. (2012) discussed the effects of mooring line inertia and damping, coupled dynamics response of truss spar in deeper water with mooring line and riser system. Kurian et al. (2015) reported a numerical and experimental study on six columns semi-submersible and showed a good agreement between the results in their restricted settings.

1.2 RESEARCH CONTRIBUTION

A current limitation of existing studies on response analysis is that all of them have focused on either numerical studies or experimental studies and both in the restricted settings of parameters and the focus has been on 'heave', 'pitch' and 'roll' degrees of freedom and less on other degrees of freedom. Also, the relationship between response of semi-submersible and its dependence on mooring line anchoring position has not been explored in-detail. We address this limitation in our work.

Our original contribution is that we conceive and present a 'Computer Simulation Model (CSM)' that is built module-by-module with each module having proper governing equations that are solved either analytically or numerically or in combination of the two, is general in its settings of parameters, is implementable in industrially standard software solutions, and is validated and verified with experimental results that are either available in literature or done for validation. This idea of the CSM is our novel and unique contribution.

This paper follows the desired focus and we believe that the presented CSM will reduce reliance on expensive and time consuming experimental studies and will allow design and development of new optimum design solutions of semi-submersible for the specific motion, cost and mooring requirements. The modular chart for Computer Simulation Module is shown in Figure. 1.

The remaining of paper is organized: Section 2 presents the detailed numerical formulation; Section 3 discusses the details of the modules; and Section 4 concludes the paper and identifies the future scope of research. Some essential details of implementation are listed in Appendix 1. A complete and detailed analysis of the results of this paper can be found in the recent thesis of first author, Vamshikrishna (2017).

2. NUMERICAL FORMULATION

The defined global axis is at the water level (X,Y,Z) and the local structural reference axis is at the 'Centre of Gravity (CoG) - (x,y,z)) - of the structure as shown in Figure. 2. Following Balrtrop (1998), and using the potential wave theory, the velocity potential for a unit amplitude incident wave is:

$$\phi_P(X,Y,Z)e^{-i\omega_I t} = \left[(\phi_I + \phi_D) + \sum_{j=1}^{6} \phi_j x_j \right] e^{-i\omega_I t} \qquad (1)$$

where ϕ_I is the incident wave potential, ϕ_D is the diffracted wave potential, ϕ_j is the potential due to j - th motion, x_j is the j - th motion in X - direction, and ω_I is the frequency of incident wave. Because of the influence of the slowly-varying motion structure has an encounter frequency effect, i.e. the excitation frequency might not coincide with the incident-wave frequency. Using Equation (1), the wave force is considered in terms of the Froude-Krylov force (i.e. F_{FK}), diffraction force (i.e. F_D), and radiation force (i.e. $F_{R_{ji}}$) and they are:

Froude-Krylov force - $$F_{FK} = -\int_{S_w} i\omega_I \rho \phi_I n_j dS_w, \qquad (2)$$

Diffraction force - $$F_D = -\int_{S_w} i\omega_I \rho \phi_D n_j dS_w, \qquad (3)$$

and

Radiation force - $F_{R_{ji}} = -\int_{S_w} i\omega_I x_i \rho \phi_I n_j dS_w$ (4)

where n_j is the generalized surface normal for j-th direction, $(n_1, n_2, n_3) = \bar{N}$, $(n_4, n_5, n_6) = \bar{r} \times \bar{N}$, S_w is the wetted surface of the body in condition of equilibrium, ρ is the density of fluid, F_{FK} is the Froude-Krylov force, F_D is the diffraction force and $F_{R_{ji}}$ is the radiation force per unit wave amplitude in the j-th direction due to the i-th motion. The potential is expressed as real and imaginary parts:

$$\phi_I = \phi_I^{\text{Re}} + i\phi_I^{\text{Im}} = \text{Real} + \text{Imaginary} \tag{5}$$

and after substituting the ϕ_R in to Equation (1), we get:

$$F_{R_{ji}} = \omega_I \rho x_i \int_{S_w} \phi_I^{\text{Im}} n_j dS_w - i\omega_I \rho x_i \int_{S_w} \phi_I^{\text{Re}} n_j dS_w \tag{6}$$

where $F_{R_{ji}}$ is the radiation force in j- th direction due to i-th motion and as the motion of body is harmonic, Equation (6) can be expressed in terms of coefficients which are in phase with the velocity and acceleration of body, e.g.:

$$F_{R_{ji}} = -A_{ji}\ddot{x}_i - B_{ji}\dot{x}_i . \tag{7}$$

Now, the added mass coefficient is:

$$A_{ji} = \frac{\rho}{\omega_I} \int_{S_w} \phi_I^{\text{Im}} n_j dS_w \tag{8}$$

and the wave damping coefficient is:

$$B_{ji} = \rho \int_{S_w} \phi_I^{\text{Re}} n_j dS_w . \tag{9}$$

2.1 EQUILIBRIUM AND STABILITY ANALYSIS

We consider stiffness matrix in the non-linear form and in the numerical simulation the entries of stiffness matrix are computed from the available analytical expressions. After the stiffness matrix is formed the body equilibrium is achieved iteratively. In each of the iterative steps entries of stiffness matrix and the entries of force vector are re-computed recursively to achieve the basic condition of body equilibrium. The initial guess of structure's position and orientation is:

$$\text{Vector } X^0 \tag{10a}$$

where $X^0 = \{x_1, y_1, z_1, p_1, q_1, r_1, x_2, y_2, z_2 .....\}$ and (p, q, r) are the finite angular rotations. In the process of iteration, the displacement at 'Step 1' is:

$$dX^{(1)} = K_h^{-1}(X^{(0)}) F_k(X^{(0)}) , \tag{10b}$$

and

$$F_k = B_{CG} - M_s g \tag{10c}$$

where B_{CG} is buoyancy at the CoG, M_s is the mass of structure, g is the acceleration due to gravity and K_h is equal to $\rho g A_w$ where A_w is the water plane area. The new position of body $X^{(1)}$ is:

$$X^{(1)} = dX^{(1)} + X^{(0)} , \tag{11}$$

and

$$\text{Termination criteria: } dX \le dX_{\text{Prescribed}} . \tag{12}$$

The iterations are continued until dX is smaller than the prescribed value ($dX_{\text{Prescribed}}$). Here the idea is to reorient the axis (user defined) to the CoG. For the static stability, meta-centric height (GM) is computed using the stiffness matrix at the condition of equilibrium by Jacobi's successive rotation method, and the positive values indicate stable equilibrium. In this paper, we consider: $GM_x \ge 2.04$ m and $GM_y \ge 8.85$ m.

2.2 FREQUENCY DOMAIN ANALYSIS (FDA)

We focus on the 'Frequency Domain Analysis (FDA)' primarily to compute the RAOs under the free floating condition for wave force only and for this the linear algebraic equations are solved. Following Barltrop (1998), the governing equation for the FDA is:

$$M_s \ddot{X} + M_a \ddot{X} + C\dot{X} + KX = F_T \tag{13}$$

where M_s is as defined before, M_a is the hydrodynamic added mass, C is the linear damping matrix, K is the total system stiffness matrix, F_T is the external force on system, X is the response function, $\dot{X}$ is the velocity of structure and $\ddot{X}$ is the acceleration of structure. The response function is:

$$X = X_0 e^{-i\omega_I t} \tag{14}$$

and the external excitation force (i.e. wave) is:

$$F_T = F_0 e^{-i\omega_I t} \tag{15}$$

where ω_I is the incident wave frequency. The solution of Equation (13) is:

$$X_0 = H_1 F_0 \tag{16}$$

where H is the transfer function which relates input forces to output response. The added mass, linear wave damping and wave forces are all frequency dependent and H_1 is:

$$H_1 = (K(\mathrm{s}) - [M_s + M_a]\omega_I^2 - iC\omega_I)^{-1}. \tag{17}$$

The RAOs at a specific point (e.g. p) is computed by:

$$X_p = T_p X_g \tag{18}$$

where X_g are the RAOs at CoG - local axis - and T_p is the translation matrix between CoG and the point p.

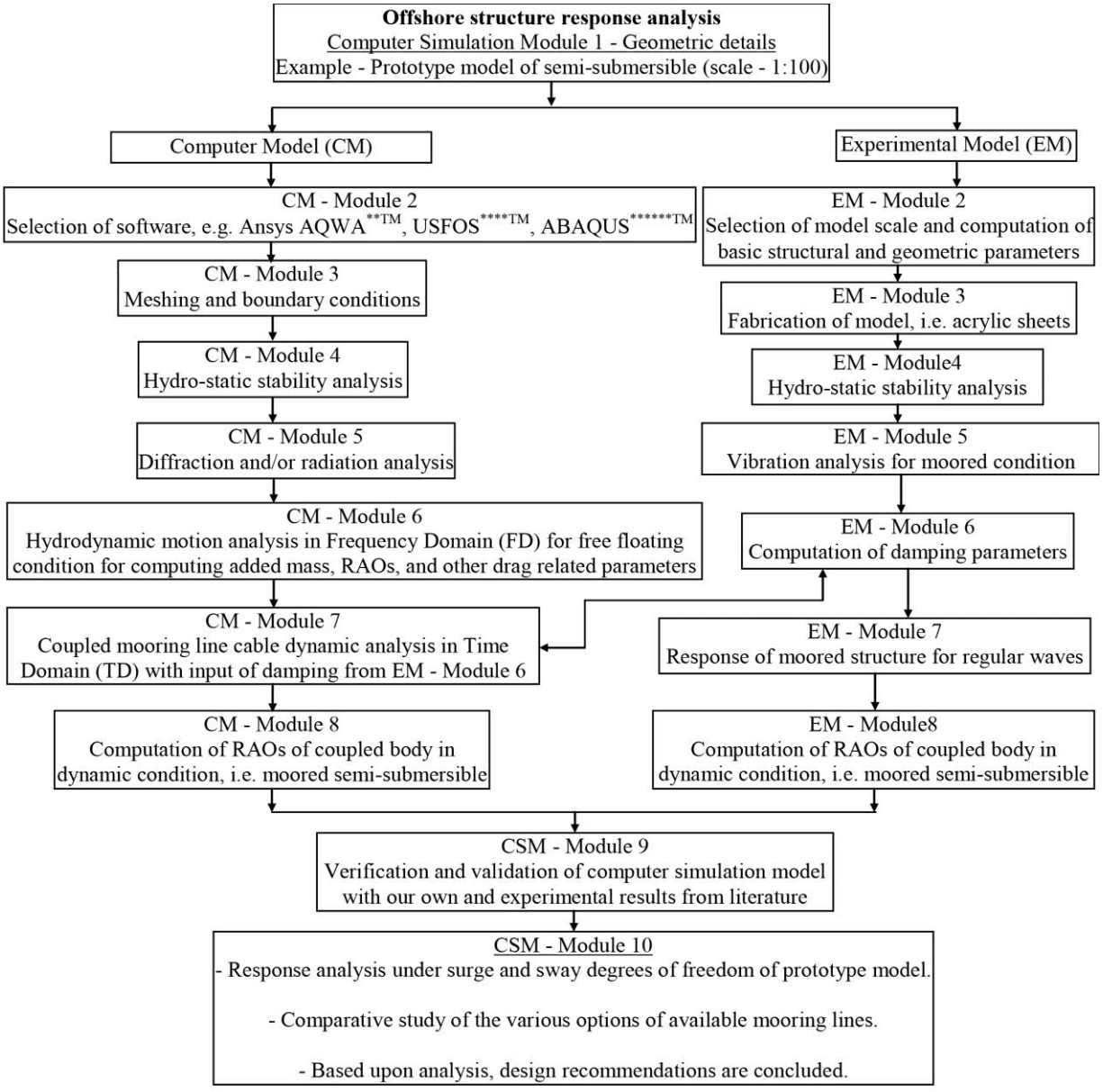

Figure 1: Modular chart for Computer Simulation Model (CSM).

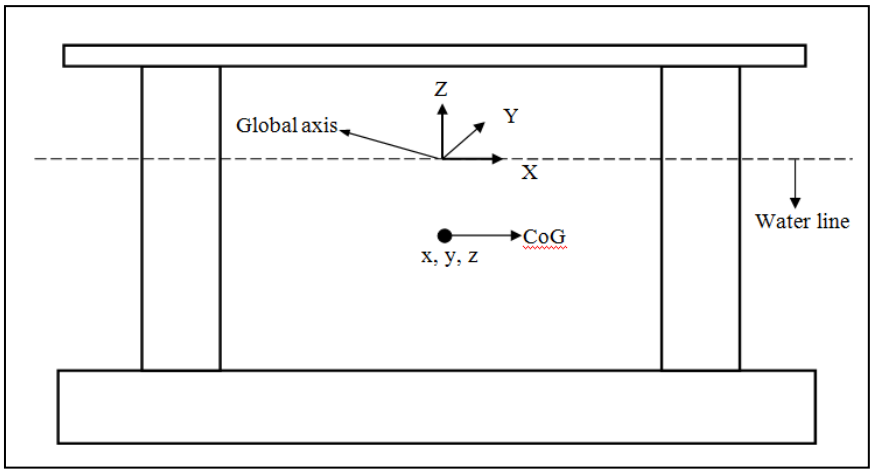

Figure 2: Schematic view showing global and local reference axes of the structural system.

2.3 TIME DOMAIN SIMULATION (TDS) FOR THE REGULAR WAVES

Following Barltrop (1998) the instantaneous displacement at time 't' is:

$$x(t) = a_{\omega_I} X_c e^{-i\omega_I t + ik_{\omega_I} x_{p1}} \tag{19}$$

where $x(t)$ is the instantaneous displacement at time t, X_c is the complex response amplitude operator at regular wave frequency ω_I with i the function representing the imaginary part, ω_I is the regular wave frequency, k_{ω_I} is the wave number corresponding to a wave frequency ω_I, x_{p1} is the distance from the origin of the wave system perpendicular to the wave direction, and a_{ω_I} is the amplitude of regular wave, $x(t)$ is the instantaneous displacement at time t. The initial velocity is:

$$\dot{x}_c(t) = i a_{\omega_I} \omega_I X_c e^{-i\omega_I t + ik_{\omega_I} x_{p1}} \tag{20}$$

where $\dot{x}_c$ is complex function for velocity. The structure is subjected to first order wave forces and the total wave frequency force is:

$$F_{wf_r} = (F_{wi} - M_a \ddot{x}_c - C\dot{x}_c) e^{-i\omega_I t + ik_{\omega_I} x_{p1}} \tag{21}$$

where

$$x = H_2 F_{wi}, \text{ and } H_2 = (K - M_s \omega_I^2)^{-1} \tag{22}$$

where $\ddot{x}_c$ is the complex acceleration, The complex acceleration is appearing because the differentiations of function can result into a complex function, e.g. $\ddot{x}$ is second differentiation of a function that consists of the complex wave force. As for the numerical instability is concerned it is stable up to medium values of added mass, with i the function representing the imaginary part, F_{wi} is the complex wave force, and F_{wf_r} is the total regular wave frequency force. A time history is created by integrating the second order differential equations of motions which requires two initial conditions (i.e. position and velocity at $t = 0$ and structure at the rest). The RAOs from FDA are used to compute the time history of wave frequency response with corresponding wave frequency and that is input in the TDS.

2.4 TDS FOR IRREGULAR WAVES

In the TDS, we consider that the total wave force is a combination of the F_{FK} and F_D with discretized wave spectrum and at any instant of time the instantaneous wave elevation is:

$$A_w(t) = \text{Real}\left\{ \sum_{j=1}^{RWCS} a_{\omega_j} e^{i(-\omega_j t + k_{\omega_j} x_{p1} + \varepsilon_j)} \right\} \tag{23}$$

where the 'Real' means that it is the real part of a complex equation, $RWCS$ is the number of 'Regular Wave Components in Wave Spectrum', $A_w(t)$ is the instantaneous wave elevation at time t, ω_j is the frequency of regular wave, k_{ω_j} is the wave number at frequency ω_j, a_{ω_j} is the amplitude of regular wave, and ε_j is the random phase frequency. At each of the time steps the total wave force is:

$$F_{wt}(t) = \text{Real}\left\{ \sum_{j=1}^{RCWS} a_{\omega_j} f_{\omega_j} e^{i(-\omega_j t + k_{\omega_j} x_{p1} + \varepsilon_j)} \right\} \tag{24}$$

where f_{ω_j} is the wave force in complex form for per unit wave amplitude at the frequency ω_j.

As has been mentioned previously, we focus on the coupled response of semi-submersible with mooring lines and in this regard the responses of semi-submersible and mooring lines are analyzed simultaneously. The dynamic effects of semi-submersible and mooring lines are included in the system equations and solved with the coupling terms. It is known that the moored semi-submersible has higher natural time periods in the surge, sway and yaw dofs as compared to the heave, roll and pitch dofs, for more details see, Newman (1974). At these natural periods, the first order excitation cannot excite the slow drift motions in steady-state conditions. Furthermore, the amplitude of excited slow-drift motions depends on the damping level involved at resonance. Hence, for a moored semi-submersible to compute the motions in surge, sway and yaw dofs the higher order spectral energies need to be computed. For the irregular waves second order oscillating wave forces exist and the oscillating frequencies are the difference between the pairs of first and second order frequencies. However, their differences are low and that can indicate the presence of wave forces with large periods that can excite the surge, sway and yaw dofs. This can lead to a large resonance motions, e.g. high drift motions.

Although, any drift motion is primarily a time dependent phenomenon, its incorporation in the modeling with a time dependent component is difficult. For computational simplicity, in the drift motion, we assume that the added mass, inertia and damping ratio are constant. Then, following Newman (1974) and Barltrop (1998), we define the equation of motion at drift frequency:

$$\left[M_s + M_a\right]\ddot{x}(t) = F_c(t) + F_w(\mathrm{t}) + F_t(\mathrm{t}) + F_h(\mathrm{t}) + F_d(\mathrm{t}) + F_{sl} \tag{25}$$

where $\ddot{x}$ is the acceleration vector, F_c is the current induced drag force, F_w is the wind induced drag force, F_t is the mooring line force, F_h is the hydrostatic force, F_d is the damping force and F_{sl} is the slowly varying drift force. In the real drift motions, the structure is subjected to first and higher order wave forces and the added mass, inertia and damping are not constant. Here, we compute the total wave force (see eq 26).

where $\ddot{x}_{\omega_j} = -\omega_j^2 x_{\omega_j}$ and $\dot{x}_{\omega_j} = -i\omega_j x_{\omega_j}$, with i as defined previously, and m_{ω_j} is the added mass at frequency ω_j, c_{df} is the damping in drift, c_{ω_j} is the damping at frequency ω_j, k_{ω_j} is the wave number at frequency ω_j, f_{ω_j} is the complex total wave force at frequency ω_j, and x_{ω_j} is the complex position at frequency ω_j. In Equation (25) the wave force is not included and later wave force is added. Now, the modified equation of motion for the drift and wave frequency is:

$$\left[M_s + M_a\right]\ddot{x}(t) = F_c(t) + F_w(\mathrm{t}) + F_t(\mathrm{t}) + F_h(\mathrm{t}) + F_d(\mathrm{t}) + F_{sl} + F_{wf}(\mathrm{t}) \tag{27}$$

For computing the response of structure at any instant of time, from Equation (27), we get:

$$x(t) = \mathrm{Real}\left\{\sum_{j=1}^{RWCS} a_{\omega_j} x_{\omega_j} e^{i(-\omega_j + k_{\omega_j} x_{p_1} + \varepsilon_j)}\right\}. \tag{28}$$

where x_{ω_j} is the complex position at frequency ω_j, i.e. the complex response amplitude.

2.5 HIGHER ORDER WAVE THEORIES

Following Chakrabarti (1987) the wave theories can be applied based on wave height and water depth. The linear wave theory results are based on sinusoidal waves with crest and through are equal in magnitude and the Response Amplitude Operators (RAOs) of a structure are computed for a fixed wave height to the time period. The non linear wave theories or higher order wave theories gives an asymmetric crest and trough with the wave line, here the crests are higher than the trough. For higher order wave theories this becomes more noticeable. The wave theories depends on three parameters the water depth (h), wave height (H) and time period of wave (T). The selection of wave theories are shown in Figure 3. As the height of crest is higher compared to trough the equations for horizontal and vertical wave particle accelerations and velocities changes and force exerted on the structure changes and the response of the structure changes.

$$F_{wf}(t) = \mathrm{Real}\left\{\sum_{j=1}^{RCWS} a_{\omega_j}\begin{bmatrix} f_{\omega_j} + \left(M_a - m_{\omega_j}\right)\ddot{x}_j \\ + \left(c_{df} - c_{\omega_j}\right)\dot{x}_{\omega_j} \end{bmatrix} e^{i(-\omega_j t + k_{\omega_j} x_{p_1} + \varepsilon_j)}\right\} \tag{26}$$

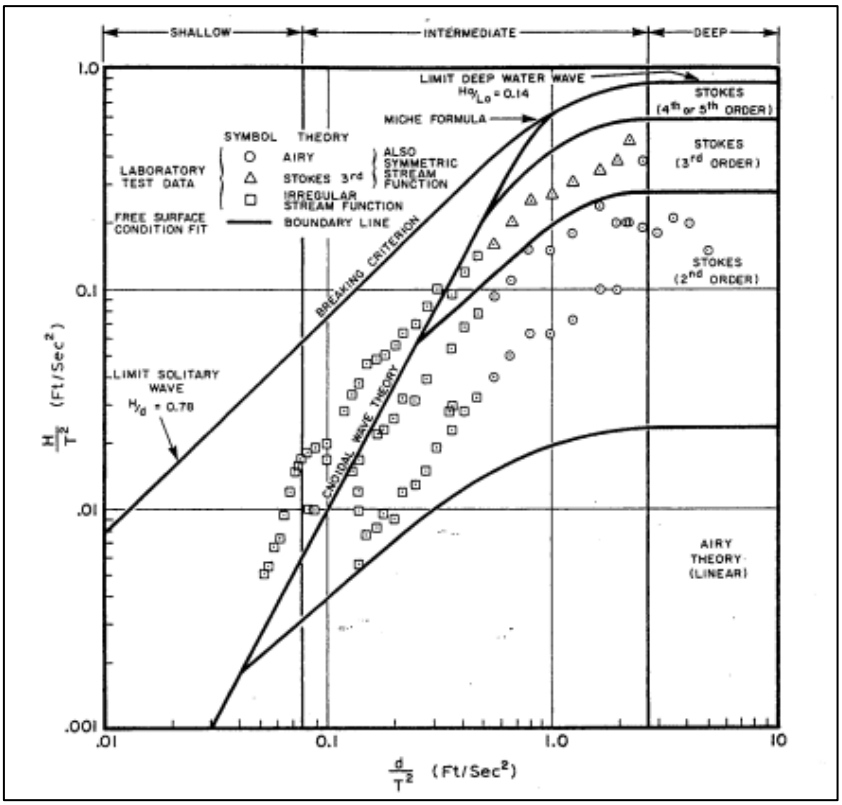

Figure 3: Suitability of the wave theories depending on H, T and d (adapted from Chakrabarti (1987)).

2.6 MODELLING OF CATENARY EQUATIONS

The coupled response of semi-submersible with mooring lines is studied through catenary equations that deal with the dynamic analysis. Following Barltrop (1998), the equations of catenary and length of mooring lines for slack condition are:

$$l_s^2 = h^2 + \frac{2T_H h}{w}, \tag{29}$$

$$l_{sus} = \sqrt{h^2\left(\frac{2T_{\max}}{wh} - 1\right)}, \tag{30}$$

$$T_H = AE\sqrt{(\frac{T_{\max}}{AE}+1)^2 - \frac{2wZ_V}{AE}} - AE, \tag{31}$$

$$X_R = \frac{T_H}{w}\sinh^{-1}\left(\frac{wl_s}{T_H}\right) + \frac{T_H l_s}{AE}, \tag{32}$$

$$T_v = wl_s, \tag{33}$$

and

$$T_{\max} = \sqrt{\left(T_H^2 + T_v^2\right)} \tag{34}$$

where l_s is the catenary length of mooring line, l_{sus} is the length of mooring line at maximum tension, h is the water depth, T_H is the horizontal component of tension, w is the submerged weight per unit length of mooring line, $T_{\max}$ is the maximum tension or total tension at the fairlead, A is the cross sectional area of mooring line, E is the modulus of elasticity, Z_V is the vertical distance between fairlead point on the structure and contact point on sea bed, X_R is the horizontal range between fairlead and contact point on sea bed and T_v is the vertical component of tension. The stiffness matrix K_g for each of the mooring lines is a 6×6 matrix and it is:

$$K_g = \begin{bmatrix} I \\ T_a^t \end{bmatrix}[K]\begin{bmatrix} I & T_a \end{bmatrix} + \begin{bmatrix} 0 & 0 \\ 0 & P_m T_a^t \end{bmatrix}, \tag{35}$$

$$T_a = \begin{bmatrix} 0 & z_f & -y_f \\ -z_f & 0 & x_f \\ y_f & -x_f & 0 \end{bmatrix}, \; \mathrm{P}_m = \begin{bmatrix} 0 & P_{z_f} & -P_{y_f} \\ -P_{z_f} & 0 & P_{x_f} \\ P_{y_f} & -P_{x_f} & 0 \end{bmatrix} \tag{36}$$

where x_f, y_f and z_f are the attachment points on structure relative to the CoG; P_{x_f}, P_{y_f} and P_{z_f} are the components of tension in the mooring line at the attachment point on structure; and T_a^t is the transpose

matrix of T_a . The force at CoG - F_g - with respect to the forces at the attachment point F_a is:

$$\left[F_g\right]=\begin{bmatrix} I \\ T_a^t \end{bmatrix}\left[F_a\right]. \tag{37}$$

In the present paper, we focus on the surge and sway motions for irregular waves. We consider a single point mass system with six dofs:

$$(M_s + m_{a11})\,\ddot{x} + C_x\dot{x} + K_{11}x = F_x(t) \tag{38}$$

and

$$(M_s + m_{a22})\,\ddot{y} + C_y\dot{y} + K_{22}y = F_y(t) \tag{39}$$

where m_{a11} is the added mass in surge direction, m_{a22} is the added mass in sway direction, C_x is the damping in x direction, C_y is damping in y direction, K_{11} is the stiffness in direction of surge, K_{22} is the stiffness in direction of sway, and $F_x(t)$ and $F_y(t)$ are the excitation forces in surge and sway directions, respectively. We write:

$$F(t) = F_{static} + F_{wave+current} + F_{drift} + F_{mooring+riser} + F_{damping} + F_{hydrostatic} \tag{40}$$

where F_{static} represents the static loads, $F_{wave+current}$ represents the first order wave loads, F_{drift} represents the drift because of wave, wind and current turbulence, $F_{mooring+riser}$ represents the forces from mooring line and riser, $F_{damping}$ represents damping force, and $F_{hydrostatic}$ represents the hydrostatic force.

2.7 MASS AND STIFFNESS MATRICES

We consider a diagonal mass matrix (M_{ij}):

$$M_{ij}=\begin{bmatrix} M+m_{a11} & 0 \\ 0 & M+m_{a22} \end{bmatrix} \tag{41}$$

where i , j = 1 to 2. The equations for added mass for each of the dofs are:

$$m_{a11} = \rho(C_{ps}\times a\times\nabla_p + C_{cs}\times b\times\pi r^2 H_s), \tag{42}$$

and

$$m_{a22} = \rho(C_{pw}\times a\times\nabla_p + C_{cw}\times b\times\pi r^2 H_s) \tag{43}$$

where ρ is the sea water density, C_{ps} is the added mass coefficient of pontoon in surge, a is the number of pontoons, C_{cs} is the added mass coefficient of column in surge, b is the number of columns, r is the radius of semi-submersible column, ∇_p is the volume displaced by the pontoons, H_s is the submerged height of column, C_{pw} is the added mass coefficient of pontoon in sway, and C_{cw} is the added mass coefficient of column in sway.

We consider the stiffness matrix of semi-submersible in the form of hydrostatic stiffness part and mooring line stiffness part. The hydrostatic stiffness for surge, sway and yaw is zero because there is no restoring force in theses dofs, and hence only stiffness from mooring line is present, i.e.:

$$K_{ij}=\begin{bmatrix} K_{11} & 0 \\ 0 & K_{22} \end{bmatrix} \tag{44}$$

where i, j =1 to 2. A unit displacement (Δx) changes the mooring force along X direction for all mooring lines and let us suppose that the initial horizontal tension in the X direction at fairlead is $T_{x\hat{i}}$ and $\Delta T_{x\hat{i}}$ is the change in tension due to the Δx , then with reference to Figure. 4, the surge stiffness (K_{11}) is estimated by taking the summation of tensions in mooring line along the X-direction and changes in tension of mooring line due to unit displacement. This results into:

$$K_{11} = \sum_{\hat{i}=1}^{n_m} \frac{(T_{x\hat{i}} + \Delta T_{x\hat{i}})}{\Delta x} \tag{45}$$

where $\hat{i}$ = 1 to n_m and n_m is the number of mooring lines.

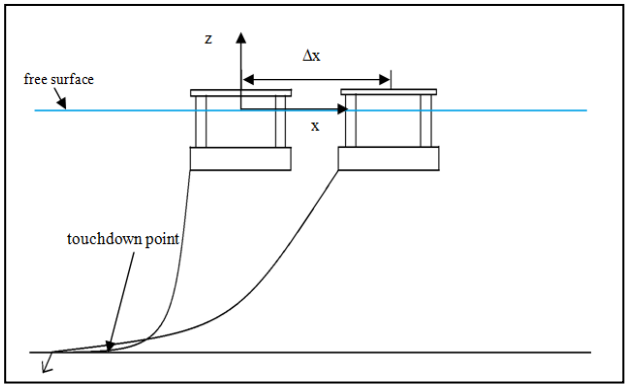

Figure 4: Displacement of the structure in X -direction.

Similar to Equations (45), for a unit displacement (Δy) the sway stiffness (K_{22}) is:

$$K_{22} = \sum_{\hat{i}=1}^{n_m} \frac{(T_{y\hat{i}} + \Delta T_{y\hat{i}})}{\Delta y} \tag{46}$$

where $T_{yi\hat{}}$ is the initial horizontal tension in Y direction of all mooring lines, $\Delta T_{yi\hat{}}$ is the change in tension for the Δy, and $\hat{i}$ = 1 to n_m and n_m is the number of mooring lines.

3. DETAILS OF THE MODULES

3.1 CM - MODULE 1 AND EM - MODULES 1 - 4

The technical details of semi-submersible used in EM and SCM are adapted from Gosain (2013) and Gosain et al. (2017), and these are listed in Table 1. The prototype to model is governed by the Froude's law of similarity. The model is fabricated with acrylic sheets (scale: 1:100) and after scaling the hydrostatic parameters are computed in MS-Excel*TM using standard procedures as defined in (Barrass and Derrett (2006)) and are checked for proper matching between prototype and model and accuracy. They match in good agreement with reasonable accuracy. The mooring line pattern is shown in Figure. 5 and 0.8 mm steel (stainless steel grade 300 series, SSS (2015)) wire is used. In the 'Ansys AQWA*TM' the option of modeling of the catenary mooring line is available. We note that the cables are taken as a catenary profile but they are not as the taut mooring line. For the sake of completeness, clarity and reproducibility we include a reference input of the catenary section in the 'Ansys AQWA*TM' as shown in Figure. 5b.

3.2 EM - MODULE 5 AND MODULE 6

In our work, the numerical modelling is based on 'Potential Theory' and that does not include the effects of viscous damping. We consider potential and radiation damping in numerical simulation and rely on experiments for computing the viscous damping parameters for better accuracy and efficient modelling. Our experiments are done on a semi-submersible model (1:100) in wave basin (30 m x 30 m x 3 m), at the Department of Ocean Engineering, IIT Madras, India. We derive the viscous damping parameters in heave, roll and pitch dofs through model testing, e.g. total damping (computed from experiments) = potential damping (computed from numerical simulation) + viscous damping. Then, the viscous damping is an input for detailed numerical modelling. The results of computation of damping are listed in Table 2. The standard logarithmic decay curves for the heave, pitch and roll dofs are shown in Figures.6a to 6c. Following, Chopra (1980), and using Figures. 6a to 6c, the damping ratios are computed:

$$\zeta = \frac{1}{2\pi}\log\left(\frac{u_{\tilde{i}}}{u_{\tilde{i}+1}}\right) \tag{47}$$

where u_i and u_{i+1} are the successive peaks in logarithmic decay curves and $\tilde{i}$ = 1 to $\hat{n}$ where $\hat{n}$ is number of peaks.

Table 1: Model and prototype details of semi-submersible.

Description	Prototype	Modified prototype	Model (1:100)
Length of pontoon	90.09 m	90 m	90 cm
Breadth of pontoon	12.12m	13 m	13 cm
Height of pontoon	6.84 m	7 m	7 cm
Diameter of column	11.74 m	12 m	12 cm
Pontoon and column spacing (transverse)	55.02 m	55.02 m	55.02 cm
Column spacing (longitudinal)	67.56 m	67.5 m	67.5 cm
Submerged height of column	19.18 m	18.86 m	18.86 cm
Meta-centric height in X (GM_x)	2.013 m	2.02	2.11 cm
Meta-centric height in Y (GM_y)	9.17 m	8.78	8.94 cm
CG from SWL	-5.8m	-6.2 cm	-6.2 cm
Longitudinal radius of gyration (r_x)	30.6 m	29.1 m	29.1cm
Transverse radius of gyration (r_y)	32.4m	32.7 m	32.7 cm
Radius of gyration in yaw (r_z)	37.2 m	38.8 m	38.8 cm
Displacement (Δ)	23699 tons	25367 tons	25.36 kg

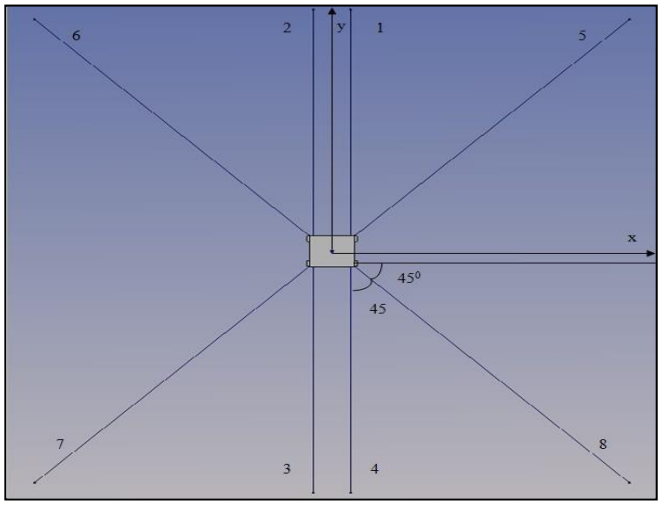

(a) Basic pattern of the mooring line for the CSM.

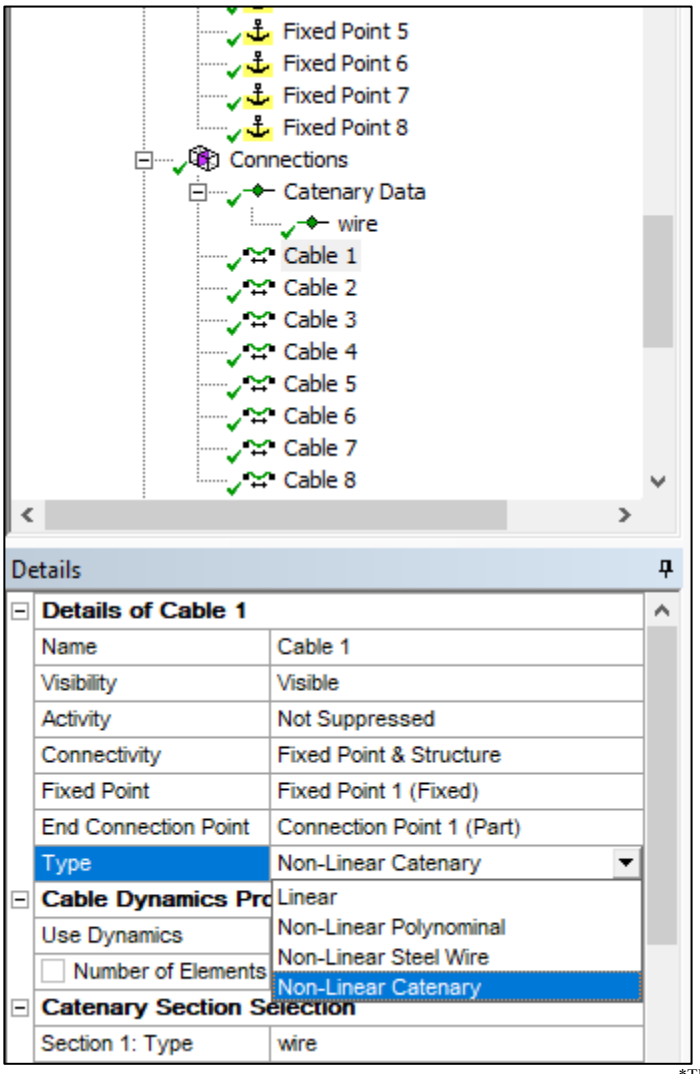

(b) A reference input of the catenary section in the 'Ansys AQWA*TM'.

Figure 5: Basic pattern of the mooring line for the CSM and a reference input of the catenary section in the 'Ansys AQWA*TM'.

Table 2: Experimental and numerical values of damping ratio.

The experimental damping ratios		
Heave	Pitch	Roll
Damping ratio %	Damping ratio %	Damping ratio %
3.390	1.910	7.040
Numerical		
1.746	0.632	6.316
Net viscous Damping		
1.644	1.278	0.724

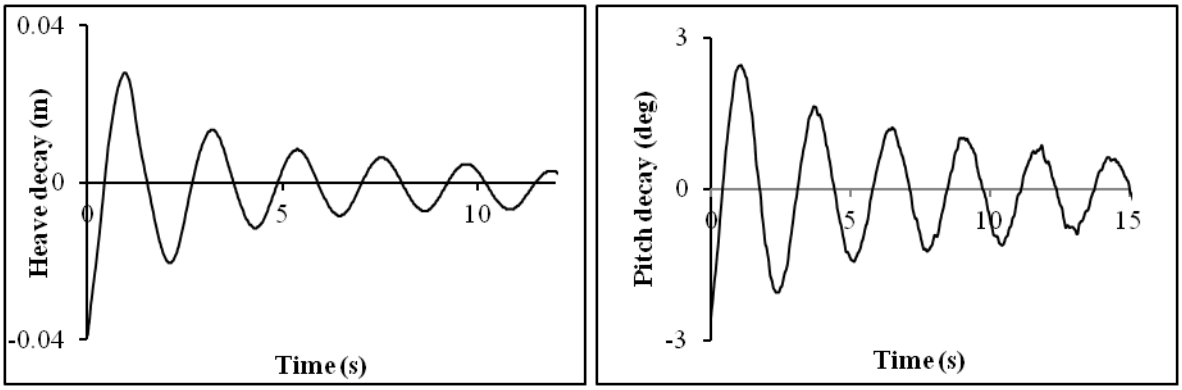

(a) Heave decay curve.

(b) Pitch decay curve.

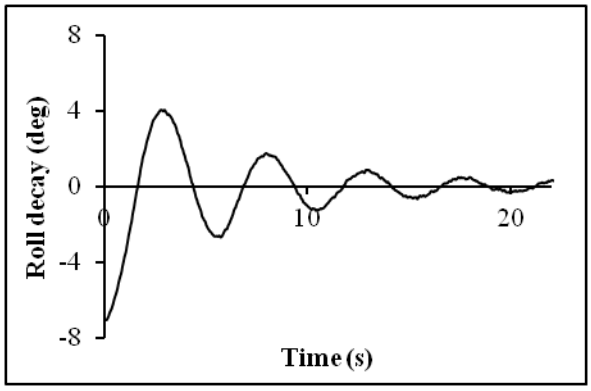

(c) Roll decay curve.

Figure 6: Standard logarithmic decay curves for the heave, pitch and roll dofs.

3.3 CM - MODULES 2 AND 3

The basic numerical formulation of Section 2 is implemented in the Ansys AQWA^{**TM} software. A scaled model of 1:100 and modified proto-type of an existing semisubmersible is studied. The 'Ansys Design Modeler (ADM)' is used for geometric modelling. The Ansys AQWA^{**TM} software has a meshing limitation of 18,000 elements, i.e. the total number of elements – in diffraction - $\leq$ 12,000. As the semisubmersible is not a structure in which the radiation responses dominate, so the remaining 12,000 elements are allocated to diffraction. These numbers include the elements below the draft line. The mesh element allocation strategy is listed in Table 3. A comparative study on the number of meshing elements is shown in Figure. 7 for the computed free floating RAOs in heave and pitch dofs. The elements above the draft line (i.e. body) are not used for the computations. From the results, we observe the following:

- The heave being a stiff dof is less sensitive to the chosen number of elements. However, the pitch is sensitive to chosen number of elements and a higher

Table 3: Mesh element allocation strategy.

S. No.	Analysis	Number of elements
1	Diffraction (Total number of elements = 12000)	Below water =12000

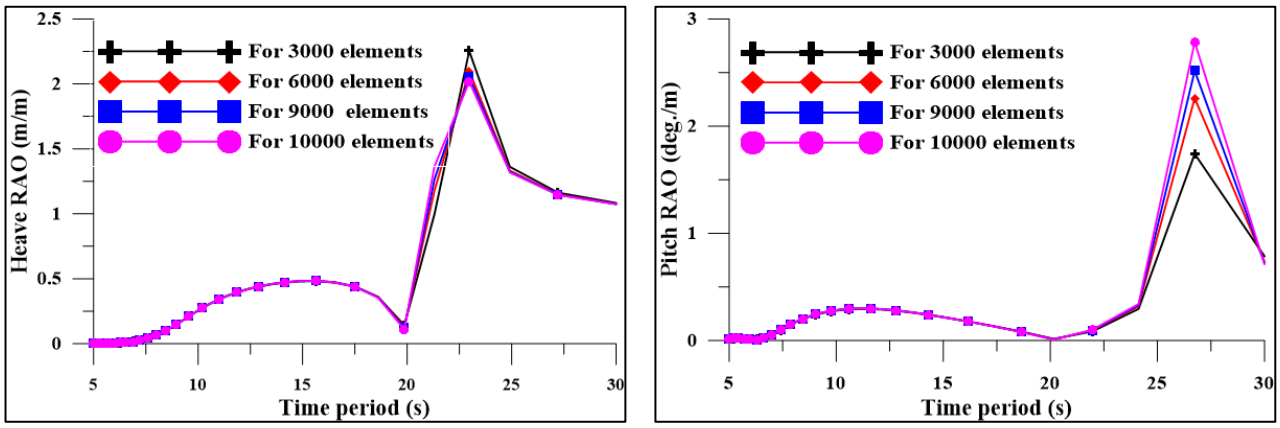

(a): Free floating heave RAO (b): Free floating heave RAO

Figure 7: Comparison of the free floating heave and pitch RAOs for different meshing elements.

number of elements are needed to capture the peak in pitch. But after the peak, the pitch response drops and it is converging. However, it is not converging at peak.

- The pattern of free floating RAOs is not sensitive to chosen number of elements and even a lower number of elements can capture the pattern of RAOs.
- The computation of peak stabilizes at around 10,000 elements, and this reinforces our mesh element allocation strategy of Table 3.

3.4 CM - MODULES 4 – 7

The diffraction and radiation analyses are done in the 'Frequency Domain (FD)' and implemented in the Ansys AWQA**TM for the free floating semi-submersible to compute the hydrostatic stability, natural frequencies of the restoring degrees of freedom, damping characteristics, added mass, stiffness matrix and free floating RAOs. After the FD analysis, the viscous damping is given as input to the Ansys AQWA**TM. The coupled mooring line cable dynamics is analyzed with regular waves of fixed wave height and increasing wave periods to obtain the responses of prototype model. The responses are analysed for each of the wave heights and results are shown for the time period of each of the waves to obtain the RAOs.

3.5 EM - MODULES 7 AND 8, CM - MODULE 8 AND CSM - MODULE 9

The verification and validation of CSM is done with experimental results. We rely upon our own experimental results and also upon the results that are available from the literature. Our experiments are conducted on scaled (1:100) model of moored semi-submersible with 0.8 mm steel wires under regular waves in the heading condition from 0.6 s to 2.8 s. The plan (i.e. top) view of semi-submersible in wave basin is shown in Figure. 8 and an image of the semi-submersible in wave basin is shown in Figure. 9. The moored semi-submersible and the mooring line numbers are shown in Figure. 10 (a) and the meshed semi-submersible is shown in Figure. 10 (b). The basic mooring line pattern is shown previously in Figure. 5. The technical details of mooring lines considered in the CSM are listed Table 4 and the diameter of mooring line is 76.2 mm. The net viscous damping listed in previously in Table 2 is given as input to the Ansys-AQWA**TM before computing the RAOs. Apart from our own experimental results, we use experimental results of Takagi et al. (1985). The comparison of computed and experimental results is shown in Figures. 11 and 12.

We can see from Figures. 11 to 12 that in-general the pattern of the CM results matches fairly well with the experiments and even peak values are in close agreement. However, the frequencies (or the time periods) do not match very closely because in computations the added masses are not computed accurately and their approximate values results in to a mismatch. This comparative study is reported in Tables 5 and 6.

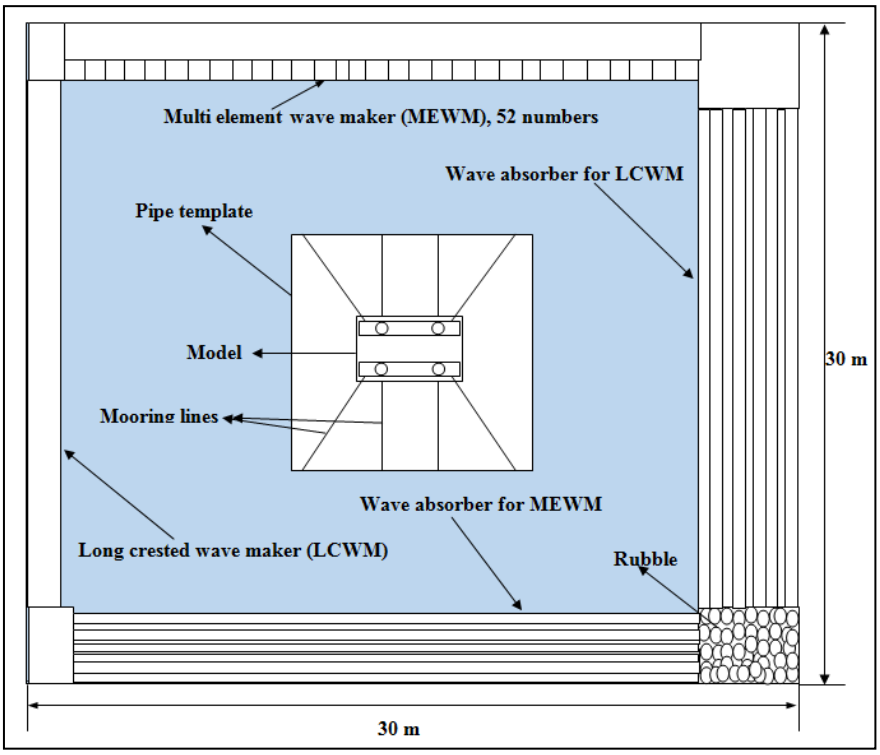

Figure 8: Schematic image of the semi-submersible model in wave basin in plan - a top view (not to the scale).

Figure 9: Image of the semi-submersible model in wave basin.

Table 4: Technical properties of the spiral stranded steel wire adapted from Barltrop (1998).

Metal wire	Stiffness/length (EA)	Submerged weight/length (w)	Breaking strength/ Catalogue break strength
Spiral stranded steel wire	$90000d^2$ N(d in mm)	$0.043d^2$ N(d in mm)	$900d^2$ N(d in mm)

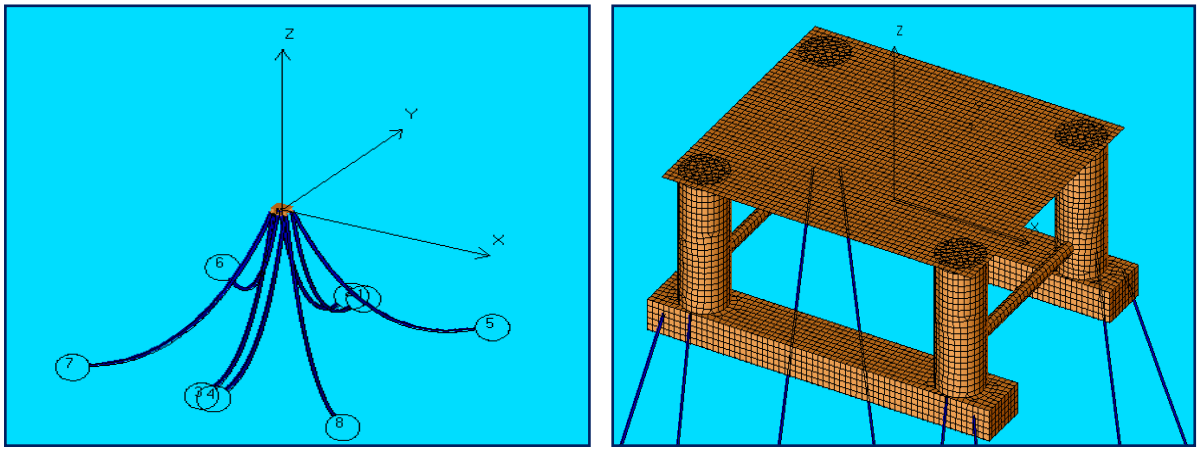

(a) Mooring line pattern. (b) Computational mesh details.

Figure 10: Mooring line and mesh details for the semi-submersible.

Table 5: Comparative study of our experimental results with CM results.

Description	Numerical	Experiment at IIT Madras	Difference
Heave RAO Peak Value (m./m)	3.2	3.1	0.1
Pitch RAO Peak value (deg./m)	3.2	3	0.2

Table 6: Comparative study of the results of Takagi et al. (1985) with CM results.

Description	Numerical	Experimental (Takagi et al. (1985))	Difference
Heave RAO Peak Value (m./m) 0 deg.	1.8	1.82	0.02
Heave RAO Peak Value (m./m) 90 deg.	1.78	1.79	0.01
Time period (s) at Peak for 0 deg.	3.05	3	0.05
Time period (s) at Peak for 90 deg.	3	3	0

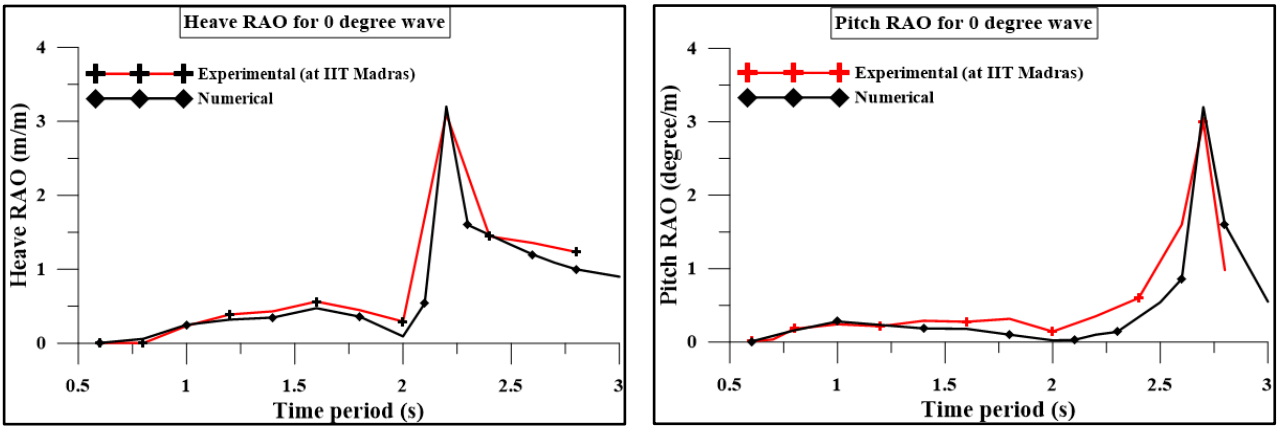

(a) Comparison of pitch RAO (b) Comparison of heave RAO

Figure 11: Comparison of experimental heave and pitch RAOs with numerical results.

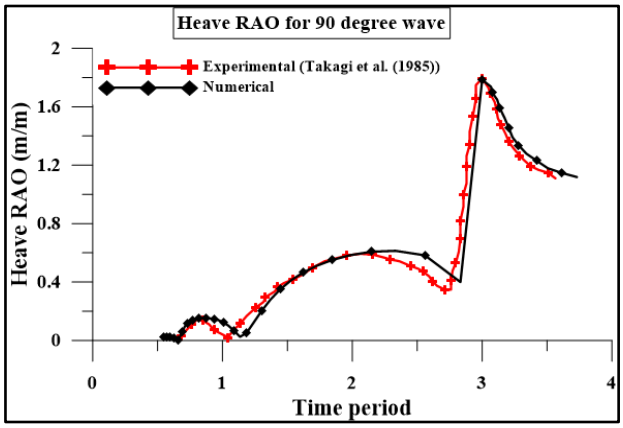

(a) Comparison of heave RAO at 0 degree wave

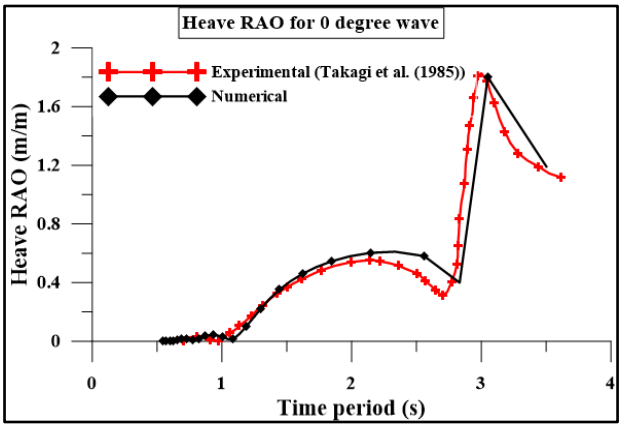

(b) Comparison of heave RAO at 90 degree wave

Figure 12: Comparison of Takagi et al. (1985) experimental heave RAOs with numerical results.

Table 7: List of the lengths of mooring lines (m) for Cases 1 to 8.

Length of mooring lines for Case 1 to Case 8 in m								
Description	Case 1	Case 2	Case 3	Case 4	Case 5	Case 6	Case 7	Case 8
Mooring line 1	1250	1325	1500	1650	1850	2100	2275	2500
Mooring line 2	1250	1325	1500	1650	1850	2100	2275	2500
Mooring line 3	1250	1325	1500	1650	1850	2100	2275	2500
Mooring line 4	1250	1325	1500	1650	1850	2100	2275	2500
Mooring line 5	1300	1550	1800	2100	2400	2700	3100	3400
Mooring line 6	1300	1550	1800	2100	2400	2700	3100	3400
Mooring line 7	1300	1550	1800	2100	2400	2700	3100	3400
Mooring line 8	1300	1550	1800	2100	2400	2700	3100	3400

3.6 CSM MODULE - 10

The TD computational analysis is done for a water depth of 1000 m to compute the effect of mooring lines on surge and sway responses with respect to the waves and currents. The computational simulation is based upon potential wave theory and incorporates the viscous damping through an input command in the simulation and acts as an additional damping.

The mooring line lengths for the Cases 1 to 8 are listed in Table 7. The natural time periods are computed in TDS after viscous damping is given as an input to the simulation and these are listed in Table 8. The change in natural periods for restoring dofs (i.e. heave, roll and pitch) is very less compared to the excitation dofs (i.e. surge, sway and yaw). The semi-submersible is given initial displacement to get the logarithmic decays in each of the dofs and the difference between two successive peaks is considered for computing the natural time periods. We see from Table 8 that there is a large difference in natural periods for the surge, sway and yaw dofs. In our opinion this is primarily because of the horizontal range of anchor points on the seabed, length of the mooring lines, horizontal and vertical forces from the mooring lines, i.e. a high horizontal range implies larger length, higher weight and higher force and along with higher stiffness. If the horizontal range increases then the length, weight and horizontal force increase and this leads to an increase in the stiffness. And, this higher stiffness leads to a decrease in the time periods for different cases. However, though the higher horizontal range of anchor point and length of mooring lines decrease the natural time period of surge, sway and yaw dofs but these only marginally affect the restoring dofs. The mooring line used for the simulation is a spiral stranded steel wire and the technical details of spiral stranded steel wire are listed previously in Table 4.

Table 8: Natural time periods (s) for Cases 1 to 8.

Description	surge	sway	heave	roll	pitch	yaw
Case 1	970	917	21.9	56.3	27.1	326
Case 2	879	803	21.9	55.8	27.1	267
Case 3	677	612	21.8	56	26.9	198
Case 4	564	501	21.8	54.9	26.8	168
Case 5	464	400	21.8	53.6	26.7	138
Case 6	338	328	21.8	52.4	26.5	118
Case 7	269	243	21.8	49.6	26.2	93
Case 8	254	228	21.8	48.8	26.18	88

The computation of displacements is done the integration of acceleration, i.e. using a '2-stage implicit' predictor-corrector scheme based on the 'Newmark-Beta method' of TMAA (2011). The integration of cable dynamics for time history solution is computed with a maximum time step of 0.1 s (inner time step) and the user input time step is outer time step. The proper specification of inner time step is important, e.g. a smaller step size increases the computational time though it can capture the steady response with better accuracy. We investigate a simple strategy: the outer time step is a divisor of inner time step and with this strategy we investigate outer time steps of 0.1 s, 0.01 s, 0.05 s, 0.001 s, and 0.005 s. The simulation time for each of the outer time steps is listed in Table 9 and user input outer time steps are listed in Table 10 and we observe that the computing time with outer time step seems to follow a linear convergence (Schatzman and Taylor (2002)) and this implies that a lower time step will result into a high computational time, e.g. the time is 1500 minutes for 0.001 step size and 15 minutes for 0.100 step size. The detailed computational results are shown in Figure 13 and they reveal that the computation of response is an 'asymptotic decay (through Stretched exponential function)' process and it does not show any further improvement beyond the outer time step that is close to inner time step. Furthermore, the computation of response function is computationally unstable and fluctuating - like any other computational computation - and it gets stabilized at around 900 s and after that results are asymptotically stable. Here, we adopt the strategy of comparing three successive peaks and if they do not show a variation of more than +/- 5 %, then we conclude that results are stable. The user input outer time steps are listed in Table 10 for Cases 1 to 8. The wave and current directions are listed Table 11 and the details of wave spectrum (i.e. JONSWAP spectrum Hasselmann et al. (1973), Wichers (2013)) are listed in Table 12.

Table 9: Simulation time (min) for each time step (s) on Computing Machine 1 (details are in Appendix A).

Time step (s)	Simulation time (min)
0.100	15
0.050	30
0.010	150
0.005	300
0.001	1500

Table 10: User input outer time steps (s).

Case description	Outer time step (s)
Case 1	0.01
Case 2	0.01
Case 3	0.05
Case 4	0.05
Case 5	0.05
Case 6	0.05
Case 7	0.05
Case 8	0.05

Table 11: Wave and current directions for analysis.

Environmental parameter	Direction (degree)
Wave	90, 120, 135, 150, and 180
Current	90, 120, 135, 150, and 180

Table 12: Wave spectrum and current details.

Wave spectrum- JONSWAP	
$H_{1/3}$ (m) - significant wave height	12.2
T_p (s) - peak time period	14
γ (Peak enhancement factor)	2.5
Current	
Depth	Velocity (m/s)
0 m	1.07
100 m	1.07
1000 m (sea bed)	0.09

The Cases 3, 4, 5, 6, 7 and 8 are run on Computing Machine 1, the Cases 1 and 2 are run on Computing Machine 2, and the details about machine configurations are given in Appendix A.

In the Ansys AQWA^{**TM}, the maximum number of 250 elements per mooring line can be modelled for cable dynamics. In our work we have considered 100 and 250 elements per mooring line for cable dynamics and it is shown in Figure 14. We conclude from Figure 14 that for cable dynamics a lower number of elements (i.e. around 100) seems to be sufficient and a higher number increases the computational time without any significant improvement in the results. Hence, we use 100 elements for all the Cases 1-8.

We study the cable dynamics in Ansys-AQWA^{**TM} with certain assumptions, e.g. cables are in either semi-taut or taut conditions, sea bed is without any slope, cable is modelled with a fixed number of elements, inline dynamics (along the line of the cable) is included, inline stiffness is limited, Morison drag forces are included, wave kinematics is ignored, current is included and sea bed friction is ignored.

As previously, we consider the global reference axis (X,Y,Z) on water surface that is exactly below the centre of the deck. We consider three synthetic fibre options and one metal option for the mooring line, e.g. synthetic fibre - polyester, aramid and HMPE, and steel metal. All the four options are considered only for Case 1 to study their response in-detail and a comparative study is reported. The steel wire ropes are used for Cases 1 to 8. The technical properties spiral stranded steel wire ropes are listed previously in Tables 4 and technical properties of the synthetic fiber wire ropes (i.e. polyester, aramid and HMPE) are listed in Table 13. The pattern of mooring lines and their

numbering are shown previously in Figures. 4 and 9 (a). The diameter of mooring line wire is 76.2 mm and it is constant for all types of the mooring lines.

The response amplitude is the average amplitude computed from the displacement time history responses. It is computed using the 'Fast Fourier Transform (FFT)' and the schematic diagram of the conversion process from displacement time history to average amplitude is shown in Figure. 15.

The Case 1 is studied in detail with four types of ropes, i.e. three fibre ropes and one spiral strand steel wire. The responses and response amplitudes are shown in Figures. 16 to 19 for different types of the mooring lines. We observe from Figures. 16 (a) and 16 (b) that the initial drift of semi-submersible is higher for all three types of the fibre wires as compared to the spiral strand steel wire. However, the steady state amplitude of response is less for the spiral strand steel wire as compared to the fibre ropes, except for the surge response at 120 degree wave and 120 degree current, where-in the polyester and aramid have higher steady state amplitude of response compared with the spiral stranded steel wire. Among the fibre and steel ropes the HMPE rope offers minimum steady state response of the semi-submersible.

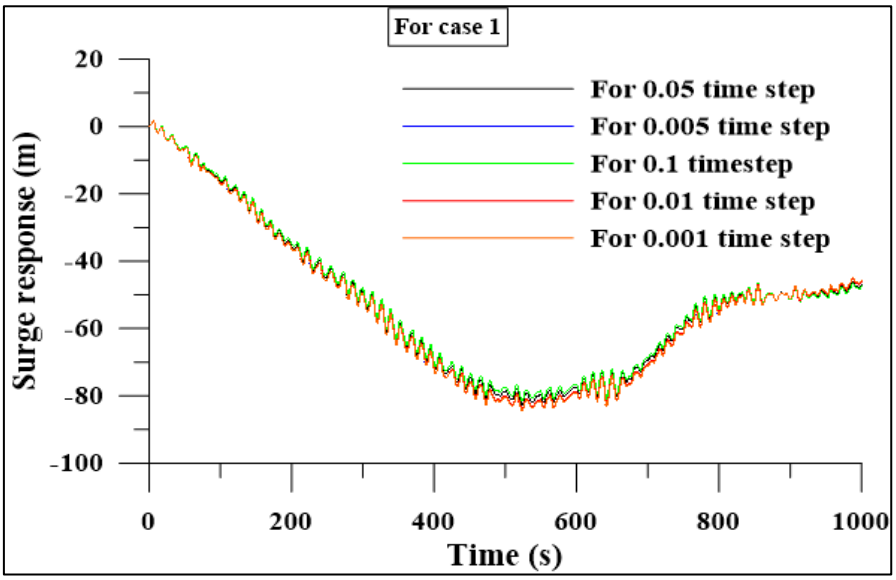

Figure 13: Comparison of time history of the surge responses of semi-submersible at different time steps on Computing Machine 1 (details are in Appendix A).

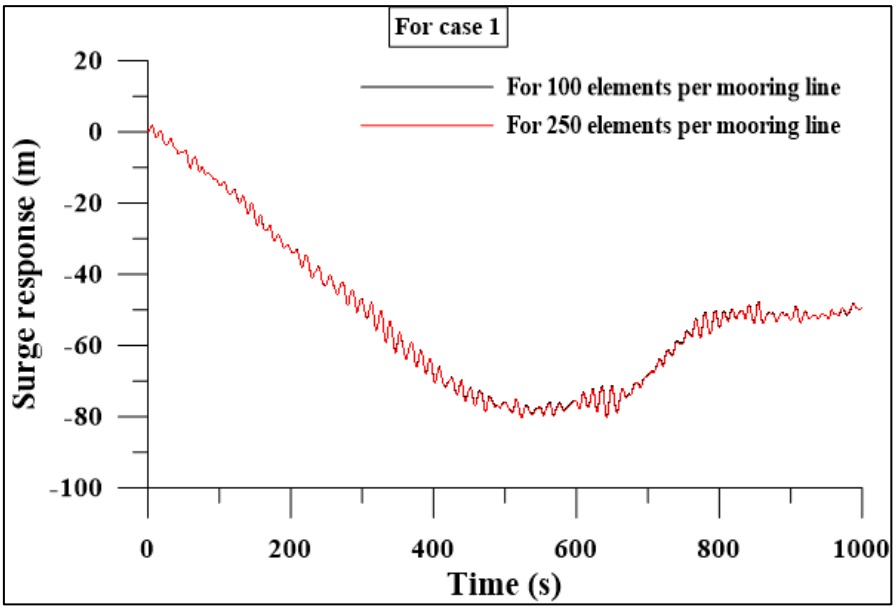

Figure 14: Comparison of time history of the surge responses of semi-submersible at 100 and 250 elements per mooring.

Table 13: Technical properties of the synthetic fibre ropes adapted from Barltrop (1998).

Synthetic fibre	Stiffness/length (EA)	Weight/length (N/m)	Breaking strength (N)
Polyester	$8000d^2$ N (d in mm)	$0.0067d^2$ (d in mm)	$250d^2$ N
Aramid	$24000d^2$ N (d in mm)	$0.00565d^2$ (d in mm)	$450d^2$ N
HMPE	$28000d^2$ N (d in mm)	$0.0062d^2$ (d in mm)	$575d^2$ N

Even though the steady state response of semi-submersible with fiber mooring lines is less, the drift is much larger, i.e. about 200 m. The drift of semi-submersible with steel mooring lines is comparatively less than half of the fiber mooring lines. As the drift is large, one side of the fiber mooring lines will be under tension and other side will be in total slack condition. This one side in total tension for the fiber mooring lines can fail due to the fatigue on other side due to oscillatory action induced by the forces of wave and current. Because of these reasons, the steel mooring lines are preferred for further analysis in our work.

The horizontal ranges of mooring lines are increased in Cases 1 to 8 in order to reduce the response of the semi-submersible in surge and sway dofs. We can see that in Case 1 the surge response is almost -80 and it is primarily because of the less horizontal distance and less stiffness of the mooring line in comparison with Case 8. Later, if we observe Figures 23 to 25 and Tables 14 to 18 then we find that the surge and sway responses are within 2 m for Case 8. Hence, in Case 8 the position is maintained and this is achieved without the application of 'Dynamic Positions System (DPS)'. From our results we conclude that the mooring line is able to maintain the position only with sufficient horizontal range and stiffness and with them being sufficient a mooring can achieve acceptable position maintenance without the DPS.

Second Order RAOs: The horizontal range of mooring lines is gradually increased from Case 1 to Case 8 and the one end of mooring line is connected to structure and the other end is connected to the seabed. The heave, pitch, roll, surge and sway RAOs are plotted based on with different wave heights and time periods while the water depth remains. Since Ansys AQWA is capable of doing Stokes second order as shown previously in Figure 4 but not other higher orders we only computed second order RAOS. In simulation the ratio of wave height to square of time period is maintained approximately 0.05.

The second order RAOs are plotted for Case 1, Case 3, Case 6 and Case 8 for 0 degree and 90 degree wave directions and these are shown in Figures 20, 21 and 22. As compared with the first order RAOs are shown previously in Figures 11(a) and 11(b) for pitch and heave the second order RAOs for have a reduced response for Case 1. The heave, pitch, surge and sway response has decreased as the horizontal distance of mooring lines are increased from Case 1 to Case 8 except for the roll response. There is not much difference is obtained for roll response when compared Case 1 with Case 8.

Irregular wave response: The Cases 1 - 8 are used to study the surge and sway responses of the structure. The detailed information on wave and current data is reported previously in Tables 11 and 12. In our model, the platform is symmetric, i.e. 0 degree is equal to 180 degree and 270 degree is equal to 90 degree and 135 degree is equal to 45 degree, etc. Hence, the wave and current directions are varied from the 90 to 180 degrees, only.

The maximum natural time period for surge is, i.e. 970 s from Table 8. We aim to compute at least 10 surge cycles with $(2 \times 3600+2800)$ s analysis and hence adopt 10,000 s in our simulation. As before, the JONSWAP spectrum (Hasselmann et al. (1973)) with different wave angles (i.e. 90 to 180 degree, 90, 120, 135, and 150, 180) and current angles (i.e. 90 to 180 degree, 90, 120, 135, and 150, 180) is used for the analysis.

The variations of surge and sway responses for Cases 1 - 8 are shown in Figures. 23 to 25 and the variations under different wave directions are listed in Tables 14 to 17. The amplitudes of surge and sway responses with respect to different natural time periods are shown in Figures. 26 (a) and 26 (b) for different Cases 1 - 8.

The natural periods are used in horizontal axis in Figures. 26 (a) and 26 (b). As each of the points in diagram suggests a Case in descending (starting with Case 8 with highest amplitude response for both surge and sway dofs) order, so a double axis is not required. We observe that the responses of surge and sway dofs depend on the 'horizontal range' of mooring lines or 'distance of anchor position' from the fairlead. As the horizontal range of mooring lines are increased the horizontal pull from the mooring line also increases and also the weight of the mooring line. The difference in responses of surge and sway for Cases 6 to 8 is significantly less, and also the natural time periods of Case 6 to 8 are less compared with others. Furthermore, they are not in the range of wave periods.

In all the eight Cases the horizontal range is increased approximately by 150 m. The catenary length of mooring lines are also increased gradually so that their catenary length remained 'the same' and this increases the horizontal force and decreases the vertical force on the platform.

From the presented results we can see that by increasing the horizontal range (i.e. from Case 1 to Case 8) decreases the natural time periods and response of the structure. For Case 8, we can see that the amplitude of sway remains below 2 m and that is very less for the semi-submersible or any moored floating structure. Importantly, we see that an increase in the horizontal range increases the horizontal force pull in the mooring lines. This increase in the horizontal force decreases the responses and causes the natural time periods to shift away from the wave frequencies even though they decrease.

Hence, we can cautiously state the surge and sway responses of semi-submersible decrease with the increase in horizontal range of mooring lines and increase with decrease in horizontal range of mooring lines. However, there are other parameters also that need to be investigated before more definitive and detailed conclusions can be drawn, e.g. vertical forces, change in the 'Center of Gravity (CoG)' of platform, and tension responses of mooring lines in the opposite directions when the platform undergoes motions in either surge or sway or both dofs. These will be explored in future.

Furthermore, the water depth considered for the simulation is about 1000 m and the surge and sway responses of semi-submersible decrease with an increase in the horizontal range of mooring lines. The minimum response is obtained when the horizontal range is about 2000 m, i.e. Cases 7 and 8. So, a simple guideline can be extracted that the response is minimum when the horizontal range is double of the water depth. This is for our particular case of the semi-submersible.

Hence, cautiously, we state that the minimum horizontal range needs to be at least 2 * water depth. And, this can serve as the design guide line for length of mooring line (i.e. fixed position on seabed from the attached point).

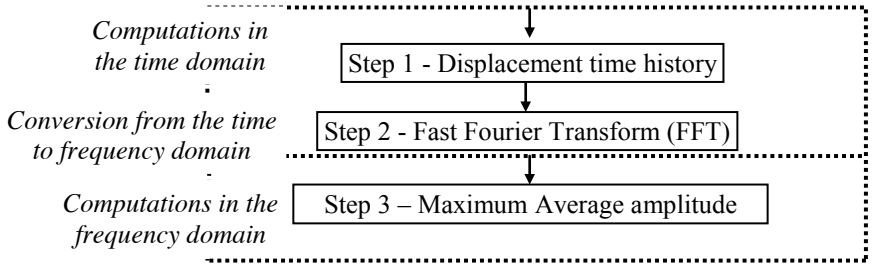

Figure 15: Schematic of the conversion process of acceleration to displacement.

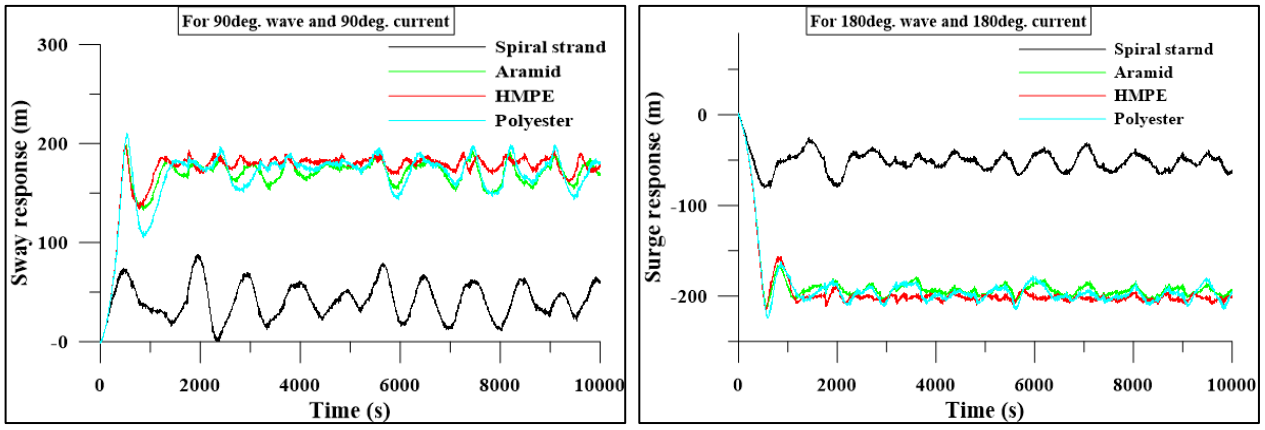

(a) Sway response time history (b) Surge response time history

Figure 16: Sway and surge time histories for different mooring line materials.

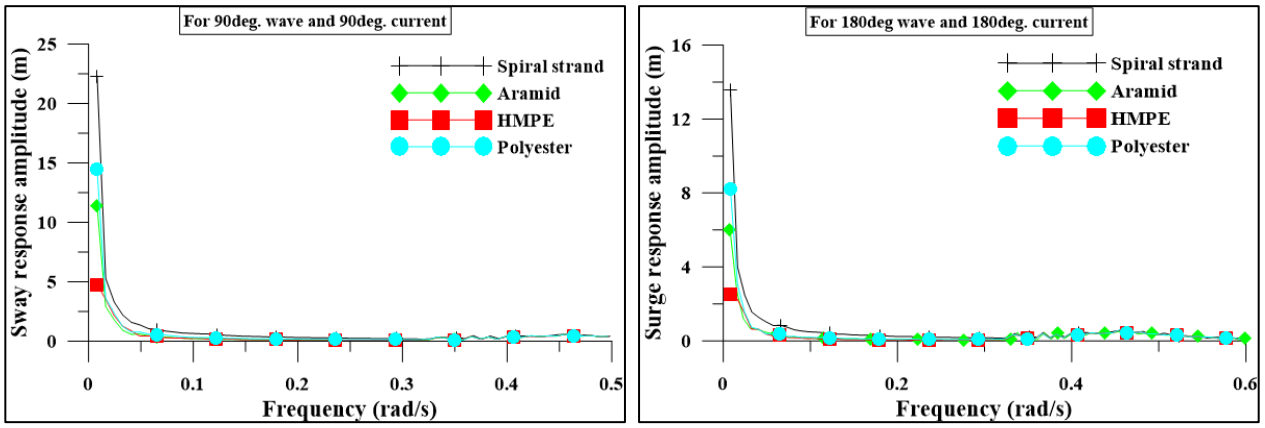

(a) Sway response amplitude (b) Surge response amplitude

Figure 17: Sway and surge response amplitudes for different mooring line materials at different current directions.

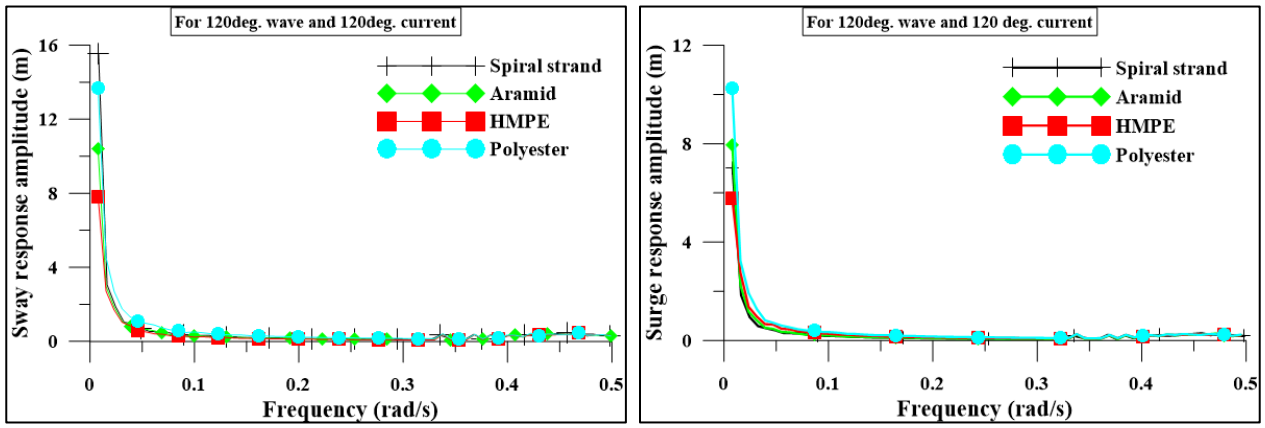

(a) Sway response amplitude (b) Surge response amplitude

Figure 18: Sway and surge response amplitudes for different mooring line materials at 120^0 wave and 120^0 current directions.

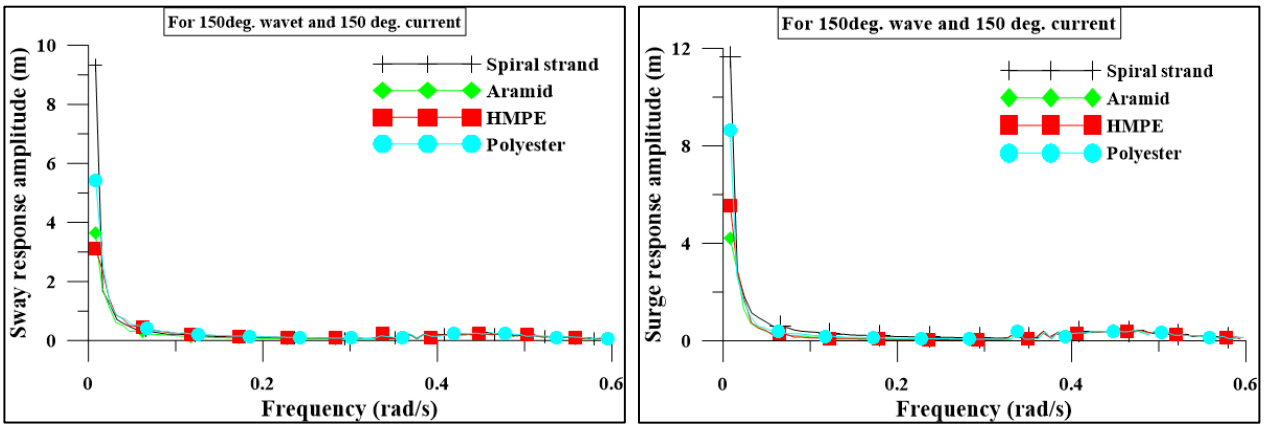

(a) Sway response amplitude (b) Surge response amplitude

Figure 19: Sway and surge response amplitudes for different mooring line materials at 150^0 wave and 150^0 current directions.

Table 14: Maximum amplitude of surge and sway responses (m) for 90^0 wave and different current directions.

90 degree wave and for different current directions										
Description	surge Amplitude					sway amplitude				
	90deg	120deg	150deg	180deg	135deg	90deg	120deg	150deg	180deg	135deg
Case 1	0.045	1.9	3.2	4.32	2.8	22.26	16	22	21	14.75
Case 2	0.04	1.5	2.6	3.36	2.3	18.78	16.2	18	16.2	14
Case 3	0.032	1	1.8	2.15	1.5	13.1	11.3	11	12	9.2
Case 4	0.0165	0.5	0.85	1	0.75	7	4.6	5.75	5.5	6
Case 5	0.01	0.34	0.55	0.7	0.49	5.9	4	5.2	4.4	5
Case 6	0.007	0.17	0.3	0.4	0.22	3.51	3	3.6	3	3.35
Case 7	0.0038	0.13	0.19	0.24	0.173	2.1	1.5	1.6	1.9	1.55
Case 8	0.003	0.13	0.19	0.23	0.172	1.8	1.3	1.3	1.5	1.35

Table 15: Maximum amplitude of surge and sway responses (m) for 120^0 wave and different current directions.

120 degree wave and for different current directions										
Description	surge amplitude					sway amplitude				
	90deg	120deg	135deg	150deg	180deg	90deg	120deg	135deg	150deg	180deg
Case 1	4.9	7	7.5	4.7	7.54	10.2	15	14.5	9.4	12
Case 2	4.2	6.6	6.3	5.1	5.8	12	15	14.5	10.8	9.6
Case 3	3.8	5.9	5	4.92	4.72	10	11.8	9	10	9.12
Case 4	2.5	2.6	4.7	3.15	3.43	5	4.2	4.9	5	5.5
Case 5	1.6	1.55	2.3	2	2.6	3.5	3.9	4.24	3.35	4.35
Case 6	0.7	0.93	1.22	0.88	1.2	2.9	2.5	3	2.22	2.65
Case 7	0.4	0.55	0.68	0.62	0.626	1.29	1.2	1.5	1.25	1.11
Case 8	0.38	0.55	0.67	0.62	0.6	1	0.9	1.2	1	0.9

Table 16: Maximum amplitude of surge and sway responses (m) for 135^0 wave and different current directions.

135 degree wave and for different current directions										
Description	surge Amplitude					sway amplitude				
	90deg	120deg	135deg	150deg	180deg	90deg	120deg	135deg	150deg	180deg
Case 1	9	10.82	10.6	11	11.75	13.57	14.2	14	12.83	12.85
Case 2	8.4	9.63	9.4	10.35	11.3	11.25	12.5	13	12.82	9.2
Case 3	6.55	6.7	8	6.85	7.77	8.6	7.6	10.1	7.25	8.8
Case 4	4.6	4.7	4.3	4.8	4.75	4.2	4.5	3.67	4.8	4
Case 5	3	3.3	2.41	3.4	3.2	3.48	3.4	3	3.42	3.2
Case 6	1.67	1.87	1.48	1.912	1.8	2.25	2.52	2	2.47	2.1
Case 7	1.05	1	0.83	1.1	1.12	1.13	1.14	0.9	1.13	1.12
Case 8	1	0.98	0.79	1.02	1.05	0.92	0.94	0.75	0.91	0.9

Table 17: Maximum amplitude of surge and sway responses (m) for 150^0 wave and different current directions.

150 degree wave and for different current directions										
Description	surge Amplitude					sway amplitude				
	90deg	120deg	135deg	150deg	180deg	90deg	120deg	135deg	150deg	180deg
Case 1	7.5	10	10.75	11.6	11.8	9.88	9.3	8.62	8.6	7.2
Case 2	8.4	8	9.5	10	9	9.4	8.84	8.2	9	8.1
Case 3	5.66	6.6	6.8	8.4	7.3	6.25	6.2	5.75	6.1	5.5
Case 4	3.2	4	4.14	4	4.25	2.78	3	2.95	2.58	2.42
Case 5	2.32	2.5	3	2.9	2.8	2.2	2.4	2.43	2.18	2
Case 6	1.52	1.38	1.78	1.6	1.42	1.6	1.55	1.6	1.57	1.42
Case 7	1	1.12	1.2	1.19	1.2	0.75	0.75	0.75	0.78	0.75
Case 8	0.95	1.08	1.1	1.18	1.1	0.62	0.6	0.6	0.62	0.6

Table 18: Maximum amplitude of surge and sway responses (m) for 180^0 wave and different current directions.

180 degree wave and for different current directions										
	surge amplitude					sway amplitude				
Description	90deg	120deg	135deg	150deg	180deg	90deg	120deg	135deg	150deg	180deg
Case 1	18.6	17.3	16.5	16	14	3.5	2.48	1.92	1.5	0.06
Case 2	16	15.3	18.2	14	14.32	2.55	1.86	1.71	1	0.05
Case 3	11.93	12.3	12.4	11	11	1.5	1.12	1.05	0.6	0.038
Case 4	8.25	6.86	5.6	6.2	5.2	0.5	0.41	0.35	0.19	0.028
Case 5	3.2	5.2	4	4	4	0.38	0.26	0.2	0.13	0.019
Case 6	2.8	3	2.85	1.75	2	0.24	0.18	0.11	0.09	0.01
Case 7	2	1.5	1.5	1.3	1.67	0.08	0.06	0.05	0.034	0.004
Case 8	1.82	1.26	1.4	1.25	1.59	0.06	0.048	0.04	0.026	0.004

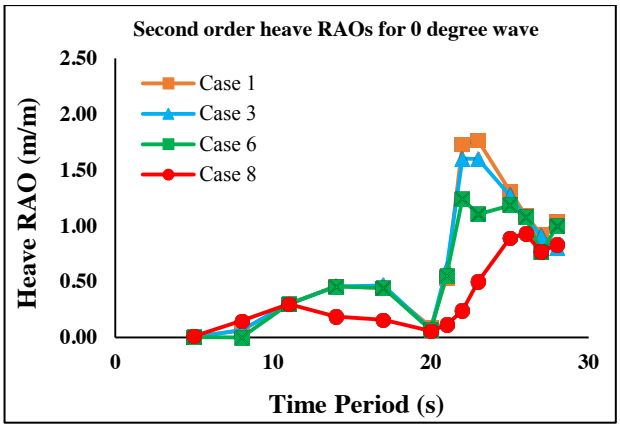

(a) Second order heave RAOS at 0 degree wave

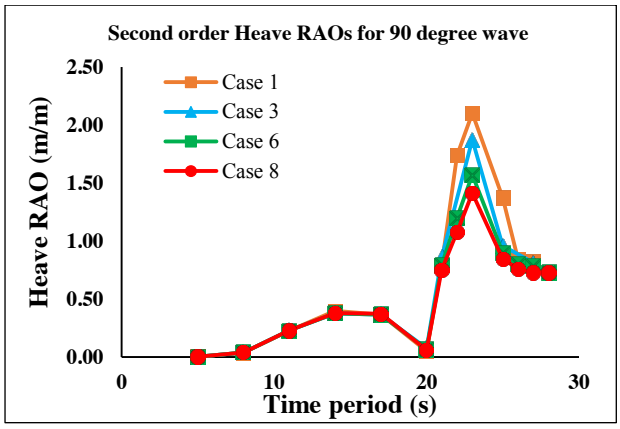

(b) Second order heave RAOs at 90 degree wave

Figure 20: Second order Heave RAOs for 0 degree and 90 degree wave directions.

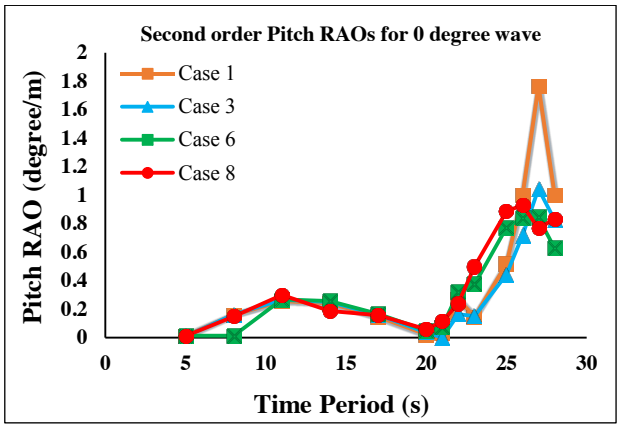

(a) Second order pitch RAOS at 0 degree wave

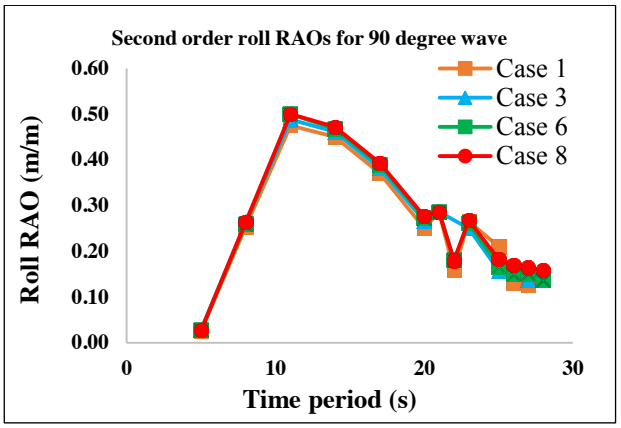

(b) Second order roll RAOs at 90 degree wave

Figure 21: Second order pitch and roll RAOs for 0 degree and 90 degree wave directions.

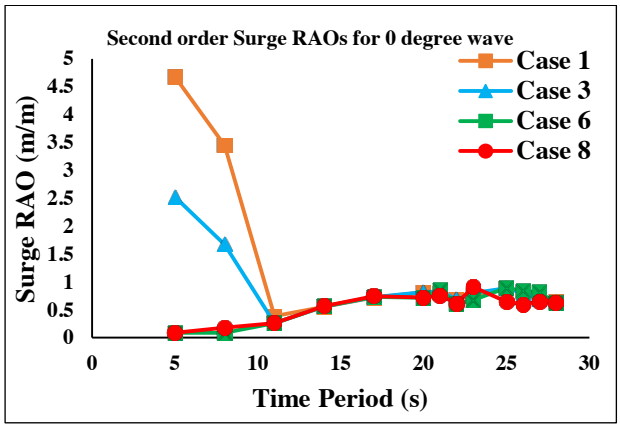

(a) Second order surge RAOS at 0 degree wave

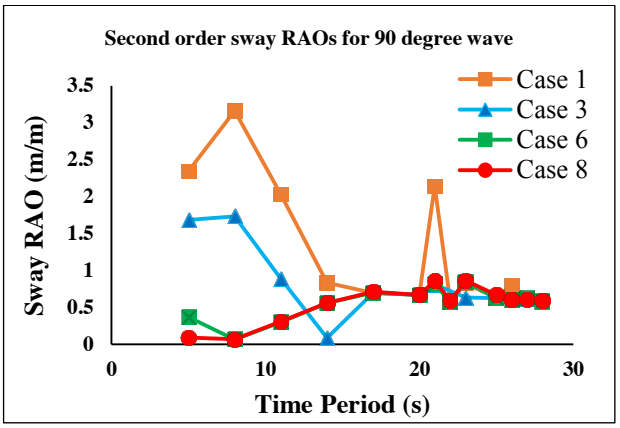

(b) Second order sway RAOs at 90 degree wave

Figure 22: Second order pitch and roll RAOs for 0 degree and 90 degree wave directions.

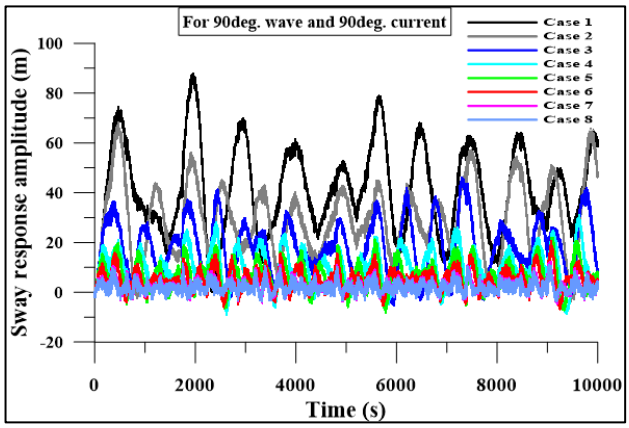

(a) Sway response time history

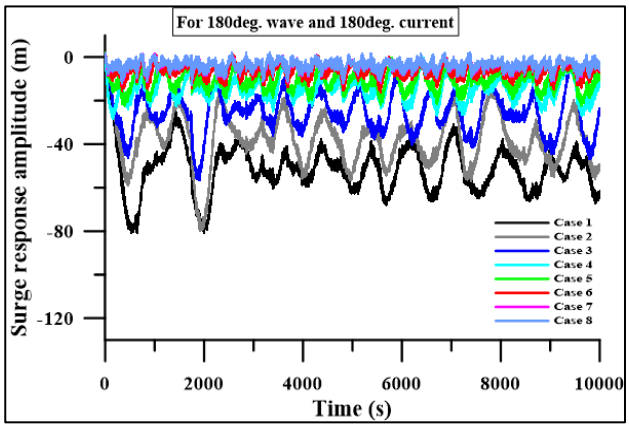

(b) Surge response time history

Figure 23: Sway and surge response time histories at different wave and current directions.

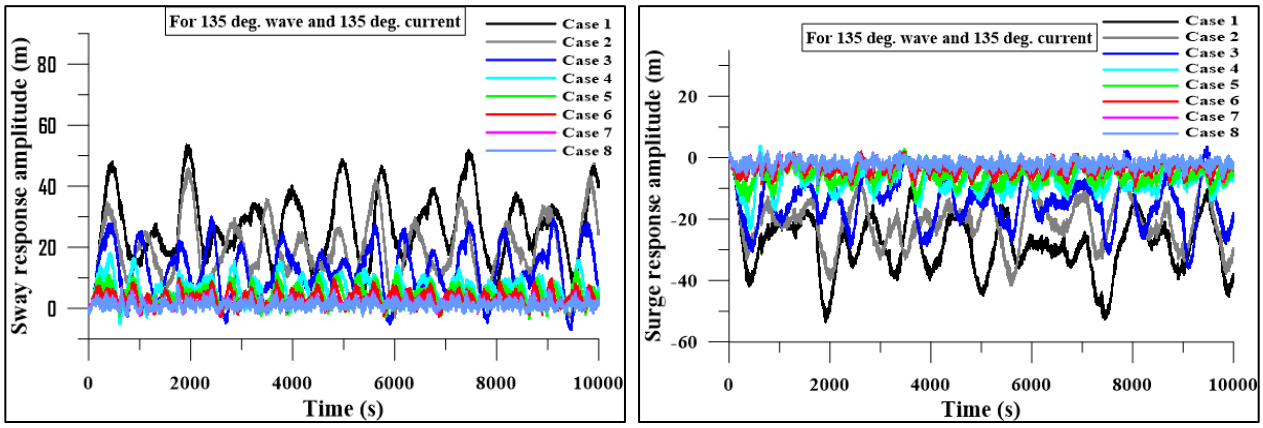

(a) Sway response time history (b) Surge response time history

Figure 24: Sway and surge response time histories at 135^0 wave and 135^0 current directions.

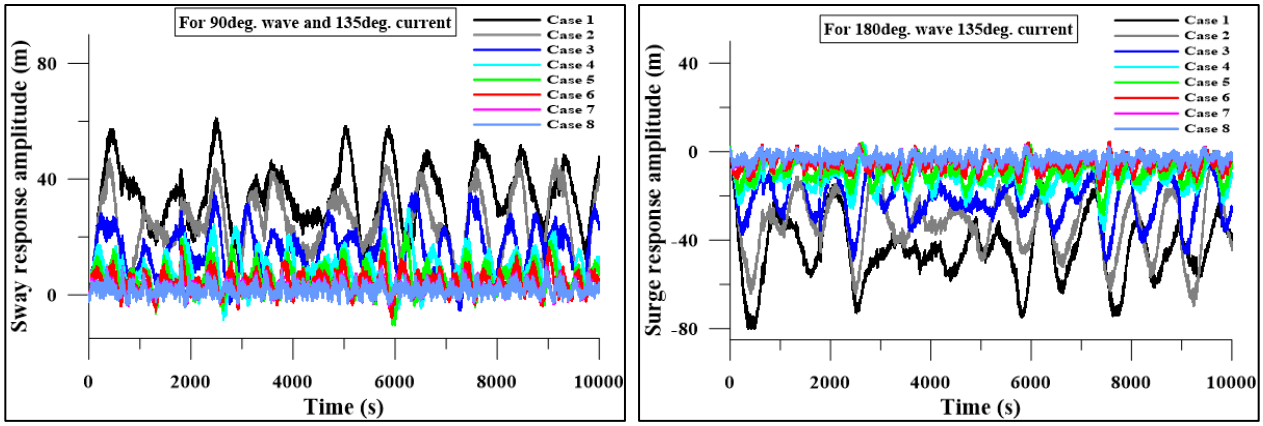

(a) Sway response time history (b) Surge response time history

Figure 25: Sway and surge response time histories at different wave and current directions.

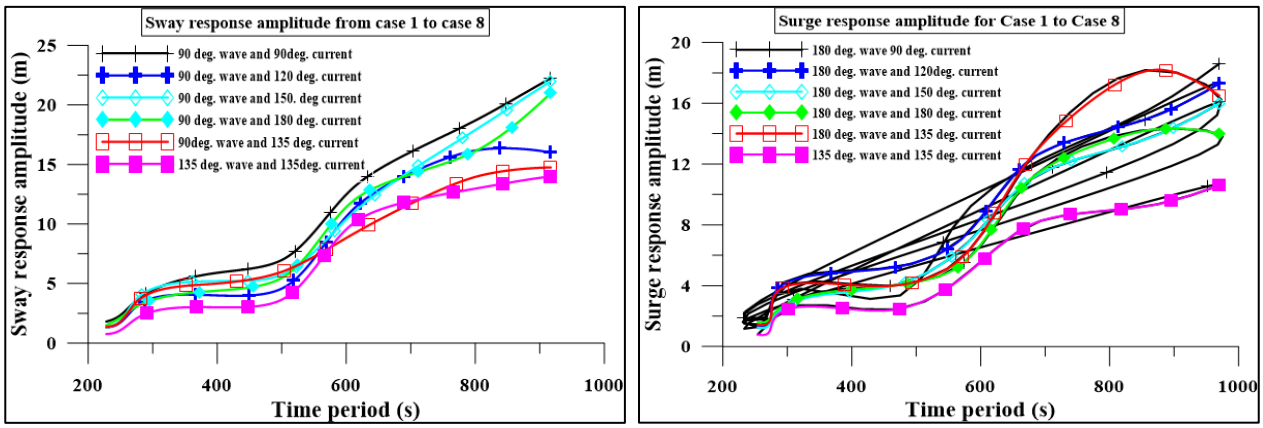

(a) Sway response amplitude (b) Surge response amplitude

Figure 26: Comparison of maximum sway and surge response amplitudes for Case 1 to Case 8 for semi-submersible under different wave and current directions.

4. CONCLUSIONS

In a computing driven world, a computer simulation based approach to design can result in design and development of new, novel, innovative and efficient designs at less cost because the reliance on expensive experiments is reduced. Our larger aim is the development of simulation based design approached and the present paper is first integrated effort in that direction. Based upon our presented work, we can conclude the following:

- A CSM for response analysis of a moored semi-submersible that is modular has been developed. The numerical simulation is based upon governing equations that are derived from basic analysis and empirical formulations available from existing research. The implementation has been in software to achieve standardized results and practice that can be adopted by the industry.
- We observe that although there is a meshing limitation (i.e. less the 12000 elements for the diffracting elements, in Ansys AQWA[**TM]), the increase in number of elements from 6000 to 10000 results into setting of the steady state responses and the results also match with the response to the semi-submersible model. Hence, the elements can be selected in this range (i.e. 6000 to 10000) for computational efficiency.
- We note that the increase in mooring line elements does show any significant differences in the response at least for our depth of operation. This is likely to be dependent upon the water depth and a more detailed investigation is needed to arrive at the selection guidelines for the number of mooring line elements.
- We note that the sensitivity analysis with different time steps implied that there is only little improvement in responses and this in our case is not significant. However, for very large floating structures this will need further investigation.
- Our modular architecture of presented model shall allow us to add more complex modules in future, e.g. structural module, operation performance module and failure module.
- Based upon our presented results, we can state that the fibre ropes offer a low steady state response compared with spiral stranded steel wires. However, because of low stiffness and tension, and less weight that allows almost floating condition for the ropes, the drift tends to be large up to 200 m for Case 1 and it is less than 100 m for spiral stranded steel wires, however the response amplitude is less for fibre mooring lines. But the metal wires offer low drift. Hence, the decision is a trade-off between drift and steady state response. Also, the cost of fibre ropes is less compared to steel wires, and they are less susceptible to corrosion, wear and tear. Based upon these parameters recent industrial applications tend to favour fibre based mooring line, e.g. Song et al. (2010) and Weller et al. (2015).
- Through the detailed simulation results of Cases 1 to 8, the natural frequency analysis showed that long horizontal range of mooring lines decreases the natural time period of surge, sway and yaw, but has a little impact on heave, roll and pitch, but from Second order RAOs there is an decrease in response for heave and pitch but roll is unchanged. Also, the responses of surge and sway depend on horizontal range of mooring lines from fairlead to anchor point and the response of semi-submersible increases in horizontal degrees of freedom when the horizontal range is less. The short horizontal range increases response and the natural time period of surge and sway. This indicates that the response of surge and sway are directly proportional to their natural time period.

We also note some of the pertinent limitations of our work as the following:

- Herein, a potential theory is used and we ignore the effects of seabed friction. The same assumptions are followed in the 'Ansys AQWA[**TM]'. Unfortunately we cannot model or input seabed friction in the 'Ansys AQWA[**TM]'. However, the tension responses at the touch down point of mooring lines can be simulated and these results can be studied and interpreted in-detail separately by considering the seabed friction. This needs to be explored in the future.
- The torsion and tension are important in the sway and surge motions and because of this they need to be simulated and analyzed. This needs to be attempted in the future.
- From our results, we can only note that the surge and sway responses depend on the mooring line length, pattern and stiffness. When we increase the horizontal ranges in Cases 1 to 8 then we observe that there is a change in the surge and sway responses and these changes are clear in Figures. 23 to 26 and Tables 14 to 18. However, to properly understand the mechanics of mooring line we note that more research needs to be done incorporating parameters like tension and pattern as they lead to a significant decrease in the surge and sway responses. This needs to be explored in future.
- As has been mentioned previously, a simulation based design approach can lead to a optimum design, e.g. we can investigate the optimum design of a low motion semi-submersible for a range of sea states with different mooring line Cases. The presented simulation model will help in that and currently this is under investigation.

5. TRADEMARKS AND COPY RIGHTS

[*]Trademark and copyright with MICROSOFT, USA. [**]Trademark and copyright with ANSYS Inc., USA. [***] Trademark and copyright with PHATAS, ECN Netherlands. [****] Trademark and copyright with USFOS,

SINTEF, Scandinavia. ***** Trademark and copyright with HAWC2, Denmark.

6. REFERENCES

1. BARLTROP, N. D. P., 1998. *Floating structures: A guide for design and analysis*, Oilfield Publications Limited 1998, vol. 2, Herefordshire, England.
2. BARRASS, B. and DERRETT, D. R. *Ship Stability for Masters and Mates*, Butterworth-Heineman, Elsevier Ltd, 2006.
3. BROWN D T, MAVRAKOS S., 1999. *Comparative study on mooring line dynamic loading*, Marine structures 1999, 12(3), 131-151.
4. BOWERS, J., IAN, M .and GILL, M., 1997. *Multivariate Extreme Value Analysis of a Moored Semi-submersible*, Marine Structures, 10(6), 443-463.
5. CHAKRABARTI S. K., 1987. *Hydrodynamics of offshore structures*, Springer Verlag.
6. CHOPRA, A. K., 1980. *Dynamics of structures - A primer*, Earth Quake Engineering Research Institute.
7. DOMALA V and SHARMA R (2018) *An experimental study on vortex-induced vibration response of marine riser with and without semi-submersible*, Proceedings of the Institution of Mechanical Engineers, Part M: Journal of Engineering for the Maritime Environment, 232 (2), 176–198.
8. GOSAIN, G. D., (2013). *Optimization model for design of semi-submersibles*, Master of Science (By Research) Thesis, Department of Ocean Engineering, IIT Madras, India.
9. GOSAIN G D, SHARMA R and TAE-WAN KIM (2017). *An optimization model for preliminary stability and configuration analyses of semi-submersibles*, Transactions of The RINA - PART A: International Journal of Maritime Engineering (IJME), Vol . 159, Part A3, Jul-Sep 2017, pp. A 249 - A 270.
10. HASSELMANN, K., BARNETT. T. P., BOUWS, E., CARLSON, H., CARTWRIGHT, D. E., ENKE, K., EWING, J. A., GIENAPP, H., HASSELMANN, D. E., KRUSEMAN, P., MEERBURG, A., MULLER, P., OLBERS, D. J., RICHTER, K., SELL, W., WALDEN, H., 1973. *Measurement of wind–wave growth and swell decay during the joint North Sea wave project (JONSWAP)*. UDC 551.466.31, ANE German Bight, Erganzunscheftzur Deutschen Hydrographischen Zeitschrift, Reihe A (8^0), Nr.12, 1973.
11. HUIJS, F. A., 2007. *The influence of steel catenary risers on the first order motions of a semi-submersible*, Proceedings of the Seventeenth International Offshore and Polar Engineering Conference, ISOPE, Lisbon, Portugal, July 1-6.
12. HUIJS, F., ROGIER DE, B., and FEIKE, S,. 2014. *Concept design verification of a semi-submersible floating wind turbine using coupled simulations*, Energy Procedia, 53, 2-12.
13. KIRK, C, L., 1985. *Resonant heave motions of semi-submersible vessels*, Ocean Engineering, 12(2), 177-184.
14. KURIAN, V. J., NG, C. Y. and LIEW, M. S., 2015. *A numerical and experimental study on motion responses of semi-submersible platforms subjected to short crested waves*, Journal of Vibration Engineering and Technologies, 3 (3), 331-344.
15. LINDENBURG, C., 2012. *Technical Report ECN-I--05-005 r11: PHATAS release 'JAN-2012b' user's manual*. Energy Research Centre of the Netherlands (ECN). Petten; website address: www.ecn.nl/publications
16. MADJID, M., QUENTIN, M., ZHEN, G., and TORGEIR, M., 2011. *Hydroelastic code-to-code comparison for a tension leg spar-type floating wind turbine*, Marine Structures, 24, 412-435.
17. MAEDA, H., TOMOKI, I., KOICHI, M. and CHANG-KYU, R., 2000. *Time-domain analyses of elastic response and second-order mooring force on a very large floating structure in irregular waves*, Marine Structures, 13 (4-5), 279-299.
18. MARCIO Y and CELSO K M. *Dynamic positioning of floating platform coupled with drilling riser*, 4^0 PDPETRO 2007, Campinas, SP, 21-24 October.
19. NEWMAN, J. N., 1974. *Second Order Slowly Varying Forces on Vessels in Irregular Waves*, International Symposium on the Dynamics of Marine Vehicles and Structures in Waves, Department of Ocean Engineering, Massachusetts Avenue, Cambridge, MA, USA, pp. 182-186.
20. SCHATZMAN, M., and TAYLOR, J., 2002. *Numerical Analysis: A Mathematical Introduction*, Oxford University Press, UK, 2002.
21. SONG, A. K., LI-PING, S., YONG, L., and QIANG, W., 2010. *Evaluation of station keeping systems for deepwater drilling semi-submersibles*, Journal of Marine Science and Applications, 9 (3), 312-316.
22. SSS., 2015. STAINLESS STEEL 300 SERIES, website address: www.nealloys.com/300_series_alloy.php.
23. SUNIL, D. K., and MUKHOPADHYAY, M., 1995. *Free vibration of semi-submersibles: A parametric study*, Ocean Engineering, 22(5), 489-502.
24. TAHAR, A., and KIM, M. H., 2008. *Coupled-dynamic analysis of floating structures with*

polyester mooring lines, Ocean Engineering, 35(17-18), 1676-1685.

25. TAKAGI, M., SHIN-ICHI, A., SEIJI, T., KUNIO, T., and NAONOSUKE T., 1985. *A comparison of methods for calculating the motions of a semi-submersible*, Ocean Engineering, 12(1): 45-97.
26. TIE-BING, S., JIAN-MIN, Y., XIN, L., and LONG-FEI, X., 2011. *Experimental investigation on wave run-up characteristics along columns and air gap response of semi submersible platform*, Journal of Hydrodynamics, 23(5), 625-636
27. TMAA, (2011). Technical Manual Ansys - AQWA v 14.0, website:www.ansys.com.
28. TMHAWC, (2015). HAWC2 Manual v 4.6, website: www.hawc2.dk.
29. TMUSFOS, (2015). Technical Manual USFOS, website: www.usfos.no
30. VAMSHIKRISHNA, D. (2017) *Studies on vortex induced responses of marine riser and moored semi-submersible*, Doctor of Philosophy (Ph.D.) Thesis, Department of Ocean Engineering, IIT Madras, India.
31. VAN SANTEN, J. A., 1985. *Approximative formulae for calculating the motions of semi-submersible*, Ocean Engineering, 12(3): 235-252.
32. WELLER, S. D., JOHANNING, L., DAVIES, P., and BANFIELD, S. J., 2015. *Synthetic mooring ropes for marine renewable energy applications*, Renewable Energy, 83, 1268-1278.
33. WICHERS, J. I., 2013. *A guide to single point moorings*, WMooring.
34. YANG, M., TENG, B., NING, D., and SHI, Z., 2012. *Coupled dynamic analysis for wave interaction with truss spar and its mooring line/riser system in time domain*, Ocean Engineering, 39, 72-87.
35. YILMAZ, O., and INCECIK, A., 1996. *Extreme motion response analysis of moored semi-submersibles*, Ocean Engineering 1996, 23(6): 497-517.

APPENDIX A

Computing Machine 1: HP Compaq Desktop PC, Model: 8200 Elite CMT PC, Processor: Intel i5 @ 3.3GHz RAM: 16GB. This is used for Cases 3, 4, 5, 6, 7 and 8.

Computing Machine 2: HP Z400 workstation, Processor: Intel Xeon @ 3.47GHz, RAM: 24GB. This is used for Cases 1 and 2.